

Value-Added Recycling of Inexpensive Carbon Sources to Graphene and Carbon Nanotubes

Sung-Joo Kwon, Hong-Kyu Seo, Soyeong Ahn, and Tae-Woo Lee*

Various methods are described here to synthesize functional carbonaceous materials (e.g., graphene and carbon nanotubes) from carbon waste for use in future optoelectronics. An ability to fabricate these materials from such inexpensive precursors would be economically beneficial. It also reviews attempts to improve the electrical properties of these materials, then discusses their practical electronic applications. Finally, future prospects for these processes are presented.

which are expensive and explosive; these disadvantages impede practical application of graphene in electronics. An alternative is to synthesize graphene and CNTs from carbon waste, which is abundant, inexpensive, and safe to handle. In this review, we focus on synthesis of graphene and CNTs from various carbon wastes, and their practical applications ranging from water purification to optoelectronic devices (Figure 1).

1. Introduction

1.1. Recycling of Carbon Wastes into Carbonaceous Conducting Materials

Household and industrial wastes pollute the environment and degrade human well-being. Natural and industrial carbon waste can be recycled to various value-added carbonaceous materials (e.g., biofuels, alcohols, and gasoline),^[1,2] so various attempts have been made to convert carbon waste to functional carbonaceous nanomaterials (e.g., graphene and carbon nanotubes (CNTs)) from carbon waste. Among the various carbon allotropes (e.g., graphene, CNTs, fullerene, amorphous carbon, and diamonds), graphene and CNTs have fascinating physical properties (i.e., outstanding electrical conductivity, optical transparency, and mechanical strength),^[3–18] and are therefore being widely evaluated for use in organic electronic devices such as organic thin-film transistors (OTFTs),^[19,20] organic solar cells (OSCs),^[21–24] and organic light-emitting diodes (OLEDs).^[25–29] To date, graphene and CNTs that are used in electronic devices have been synthesized mostly by chemical vapor deposition (CVD)^[30,31] or arc discharge^[32] that use high-purity carbon-based precursor gases (e.g., CH₄ and C₂H₂),

1.2. Structure and Properties of Carbonaceous Functional Materials


Graphene is an atomically thin layer of carbon atoms in a hexagonal network. Because graphene is composed of sp²-hybridized chemical bonds, it has unique electrical, optical, and mechanical characteristics. Exfoliated graphene has high electron mobility ($\approx 10\,000\text{ cm}^2\text{ V}^{-1}\text{ s}^{-1}$),^[3] and transistors that use this graphene show ambipolar characteristics. Even in suspended graphene, ultrahigh electron mobility ($>200\,000\text{ cm}^2\text{ V}^{-1}\text{ s}^{-1}$) has been reported (Figure 2a).^[38] Graphene's intrinsic zero bandgap and its easy tunability offer wide applications ranging from electrodes to semiconductors. Single-layered graphene has high optical transmittance (OT) ($\approx 97\%$), which decreases by $\approx 2.3\%$ per layer as the number of stacked graphene layer increases (Figure 2b).^[39] Defect-free graphene has a breaking strength of 42 N m^{-1} , which indicates that it has a Young's modulus of $\approx 1100\text{ GPa}$ and an intrinsic strength of $\approx 125\text{ GPa}$ (Figure 2c).^[40]

Since CNTs were first reported by Iijima,^[41] numerous studies on CNT have been performed due to its unique electronic and mechanical properties. CNTs are cylindrical structures of graphite with very high ratio of length (up to several micrometers) to diameter (a few to several tens of nanometers).^[42] CNTs also have sp²-hybridized bondings, which causes unique electronic and mechanical properties.^[43] CNTs can be classified into single-walled CNTs (SWCNTs) and multiwalled CNTs (MWCNTs), where MWCNTs are composed of concentric SWCNTs. Field-effect transistors (FETs) that had CNT channels showed field-effect mobility of $\approx 79\,000\text{ cm}^2\text{ V}^{-1}\text{ s}^{-1}$ (Figure 2d).^[44] CNT ropes have an average strength of $13\text{--}52\text{ GPa}$ with a Young's modulus of $320\text{--}1470\text{ GPa}$ (Figure 2e).^[45] In addition, CNT layers can be deposited uniformly with controlled thickness, and the layer has optical transparency $>70\%$ over the visible spectrum (Figure 2f).^[46] These outstanding electrical, optical, and mechanical properties of graphene and CNTs have stimulated numerous attempts to use these substances in flexible and stretchable optoelectronics.^[3–9]

S.-J. Kwon, Dr. H.-K. Seo, S. Ahn
Department of Materials Science and Engineering
Pohang University of Science and Technology (POSTECH)
Pohang, Gyungbuk 790-784, Republic of Korea

Prof. T.-W. Lee
Department of Materials Science and Engineering
Seoul National University
1 Gwanak-ro, Gwanak-gu, Seoul 08826, Republic of Korea
E-mail: twlees@snu.ac.kr, taewlees@gmail.com

Prof. T.-W. Lee
Nano Systems Institute (NSI)
Institute of Engineering Research
Research Institute of Advanced Materials
Seoul National University
1 Gwanak-ro, Gwanak-gu, Seoul 08826, Republic of Korea

 The ORCID identification number(s) for the author(s) of this article can be found under <https://doi.org/10.1002/adsu.201800016>.

DOI: 10.1002/adsu.201800016

2. Graphene

2.1. Conventional Synthetic Methods for Graphene

Mechanical exfoliation can simply obtain small graphene sheet from graphite. Graphite is composed of numerous graphene sheets, which are held together by van der Waals force. Because the van der Waals force between the graphene sheets is weak, the adhesive force of scotch tape is strong enough to exfoliate graphene sheets from graphite. Repeating this peeling process yields graphene sheets (Figure 3a).^[47,48] To date, mechanical exfoliation has yielded graphene with the best quality,^[47] but this method has poor yield and cannot prepare sizable graphene; thus, it is not a suitable method in practical applications. Several methods have been developed to improve the productivity of graphene.

Chemical reduction exfoliates and stabilizes the graphene sheet in solution form (Figure 3b).^[49,50] Chemical reduction is solution-processable, so it can be used to produce massive quantities of graphene. In chemical reduction, graphite is chemically modified to graphene oxide (GO) by the Hummers method.^[49] During the oxidation process, hydrophilic oxygen-related functional groups (e.g., epoxide and hydroxyl) formed, so water intercalates between the graphene oxide sheets; then application of mechanical energy (e.g., sonication and centrifugation) to GO suspension readily exfoliates the graphene sheets. Although GO itself is not electrically conductive, thermal annealing or treatment with chemical reducing agents (i.e., N_2H_4) converts GO to reduced GO (rGO), which is electrically conductive. Reduction of GO removes oxygen-related functional groups, so the hexagonal graphitic network is restored and conductivity is increased. However, graphene obtained by using chemical reduction still retains numerous oxygen-related functional groups (e.g., carbonyl and carboxyl) and defects, so its electrical conductivity is too low to be useful in practical electronic applications.

CVD uses a catalytic metal (e.g., Cu, Ni, Co, and Ru)^[51] and can overcome disadvantages of chemical reduction. In CVD, carbon precursors (e.g., CH_4 and C_2H_2) are injected into a quartz tube at high temperature ($\approx 1000^\circ C$); they decompose to carbon atoms on a catalytic metal surface and assemble into a graphene layer (Figure 3c).^[51,52] The mechanism of graphene growth is affected by the carbon's solubility in the catalytic metal.

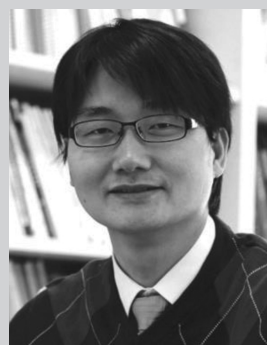
Typical catalysts for graphene synthesis are Cu and Ni, which have limited ability to dissolve carbon. Importantly, Cu has much lower carbon solubility than Ni does. Due to the low carbon solubility of Cu, very little of the carbon released by decomposition of the carbon source can diffuse into the Cu, instead, and the graphene is adsorbed to the surface and grows by surface diffusion. When the surface is completely covered, growth ceases because the carbon source can no longer react with the catalyst; as a result, monolayer graphene is produced. In contrast, Ni can dissolve more carbon than Cu can; during subsequent cooling the carbon precipitates to the surface and assembles into multilayered graphenes.^[51] However, the number of layers cannot be readily controlled. The catalytic metal substrate is removed by a chemical etchant, which is then removed by rinsing in water; synthesized



Sung-Joo Kwon received his B.S. (2013) in Materials Science and Engineering from Pohang University of Science and Technology (POSTECH), Republic of Korea. He is a graduate student in POSTECH since 2013. His current research work is focused on graphene electrodes for flexible organic optoelectronic devices.



Hong-Kyu Seo received his B.S. (2011) in the department of Information Display from Kyung-Hee University and Ph.D. (2017) in Materials Science and Engineering from Pohang University of Science and Technology (POSTECH), Republic of Korea. He is currently working as a senior researcher in Samsung Advanced Institute of Technology (SAIT), Republic of Korea (2017-present). His research focuses on organic and organic-inorganic hybrid electronics based on graphene and transparent conductive electrodes for flexible displays, and solid-state lightings.



Tae-Woo Lee is an Associate Professor in Materials Science and Engineering at the Seoul National University, Korea. He received his Ph.D. in Chemical Engineering from the KAIST, Korea in 2002. He joined Bell Laboratories, USA, as a postdoctoral researcher and worked at Samsung Advanced Institute of Technology (2003-2008). He was an Associate Professor in Materials Science and Engineering at the Pohang University of Science and Technology (POSTECH), Korea, until August 2016. His research focuses on printed flexible electronics based on organic, carbon, and organic-inorganic hybrid perovskite materials for displays, solar cells, and bio-inspired neuromorphic electronics.

graphene can be transferred to a target substrate by using supporting polymers. However, all of these methods that use purified gaseous precursors are expensive. The high cost impedes development of practical graphene-based devices for everyday use.

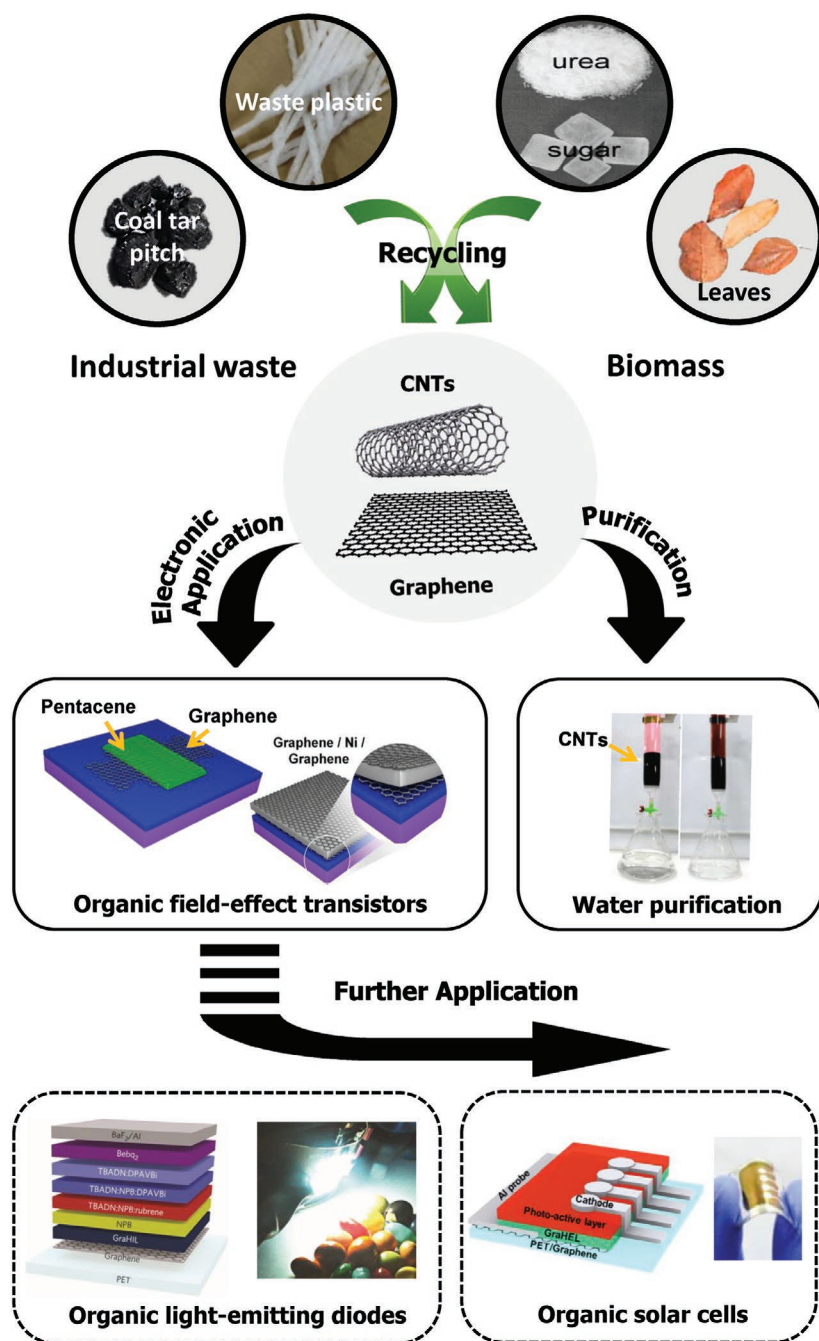


Figure 1. Synthesis of graphene and CNTs from inexpensive feedstocks of industrial and biomass wastes and its practical applications. Top) Reproduced with permission.^[33–36] Copyright 2015, Nature Publishing Group, Copyright 2014, Elsevier, Copyright 2013, American Chemical Society, Copyright 2015, Elsevier; middle) Reproduced with permission.^[33,37] Copyright 2015, Nature Publishing Group, Copyright 2012, American Chemical Society; bottom) Reproduced with permission.^[22,25] Copyright 2012, Nature Publishing Group, Copyright 2014, IOP Publishing.

2.2. Synthesis of Graphene Using Carbon Wastes

Graphene synthesis from inexpensive carbon sources has been attempted. The following sections present reported methods to synthesize graphene from wastes, and compares its characteristics (Table 1).

2.2.1. Pyrolysis

Pyrolysis is thermal decomposition of materials at elevated temperatures in an inert atmosphere. This simple and inexpensive method has been used to synthesize graphene from camphor leaves.^[36] Purification, drying, and brief high-temperature annealing yielded a raw material, which was immersed in a trichloromethane solution containing D-tyrosine, which forms π - π interactions with graphene to yield few-layered graphene (FLG) that can be recovered by centrifugation (Figure 4a). The FLG formation from leaves was confirmed using transmission electron microscopy (TEM) (Figure 4b); the thickness of FLG was determined by Atomic force microscopy (AFM) to be 2.37 nm, which corresponds to about seven layers (Figure 4c). Raman spectroscopy is a nondestructive tool to identify the number of layers and structural disorder of graphene, which is also a basic unit for CNTs. A Raman spectrum of graphene includes three prominent bands: i) the D band ($\approx 1350\text{ cm}^{-1}$) indicates the density of defects and disordered regions; ii) the G band ($\approx 1580\text{ cm}^{-1}$) represents the stretching of bonds between sp^2 -hybridized carbons, and quantifies the crystallinity of sp^2 -hybridized carbon networks; and iii) the 2D band ($\approx 2700\text{ cm}^{-1}$) is related to the second order of zone-boundary phonons.^[61] A low ratio of the intensities of the D (I_D) and G (I_G) bands is evidence of high-quality graphene. In Raman spectra, the average I_D/I_G of graphene from camphor leaves was 0.99 (Figure 4d), which was not as low as that of pure graphene. In addition, no sharp D, G, or 2D peak was observed; the absence might be caused by residual chemical groups on the FLG surface, or by multilayer structural defects.^[62] This study demonstrated that pyrolysis of inexpensive biomass (here, camphor leaves) is feasible method to synthesize large-area graphene at low cost.

Graphene has also been synthesized from plants and flower petals.^[53] Lotus petals have been used as carbon sources because the carbon-carbon bonds of the constituent cellulose and hemicellulose could undergo cleavage and molecular rearrangement at high temperature in an anaerobic environment to form graphene.^[55,63] Graphene or Ni-decorated graphene, respectively, was formed when petals or petals soaked in NiCl_2 solution were annealed at $800\text{ }^\circ\text{C}$ for 30 min under Ar atmosphere. The quality of graphene was improved by increasing the temperature to $1600\text{ }^\circ\text{C}$. Scanning electron microscopy (SEM) images of the graphene formed at $1600\text{ }^\circ\text{C}$ (Figure 5a) and graphene-Ni (Figure 5b)

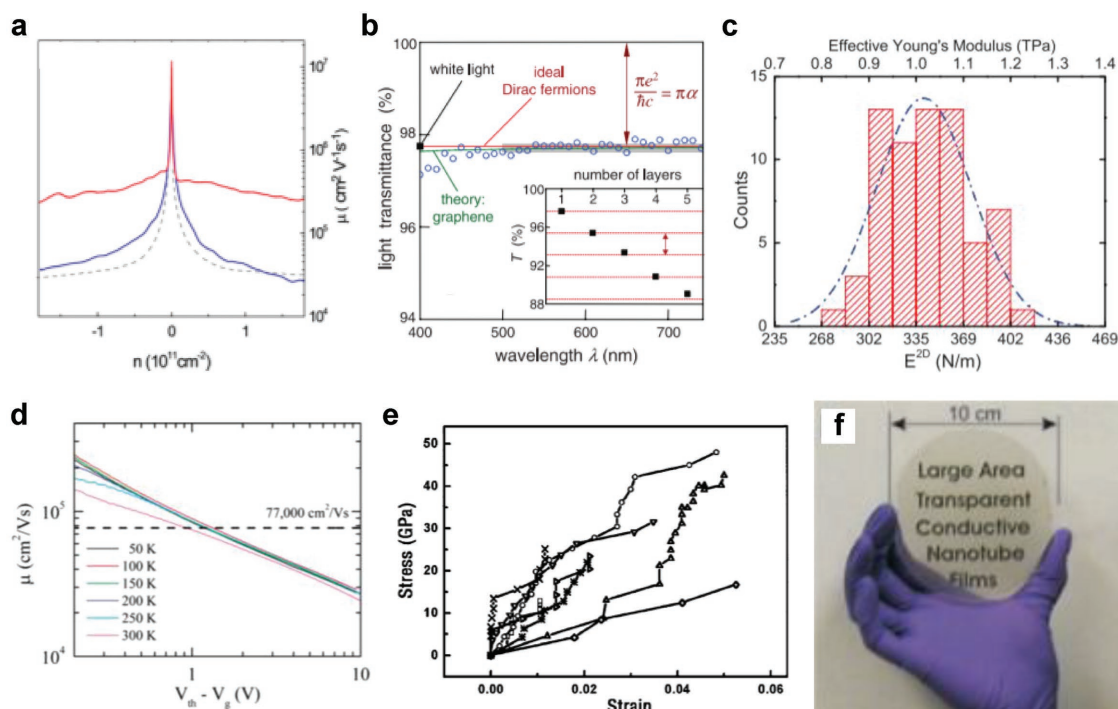


Figure 2. a) Charge carrier mobility of suspended graphene versus charge carrier density calculated from field-effect transistors that use suspended graphene before (blue) and after (red) current annealing, Reproduced with permission.^[38] Copyright 2008, Elsevier. b) Transmittance of single-layered graphene versus wavelength of light. Inset: transmittance of white light as a function of a number of graphene layers. Reproduced with permission.^[39] Copyright 2008, American Association for the Advancement of Science. c) Histogram of elasticity of graphene. Reproduced with permission.^[40] Copyright 2008, American Association for the Advancement of Science. d) Charge mobility versus gate voltage in FET based on CNTs at various temperature. Reproduced with permission.^[44] Copyright 2004, American Chemical Society. e) Stress versus strain curves of various single-walled nanotubes. Reproduced with permission.^[45] Copyright 2000, American Physical Society. f) Photograph of large-area carbon nanotube film. Reproduced with permission.^[46] Copyright 2004, American Association for the Advancement of Science.

revealed a very thin graphene layer that could be penetrated by electrons, and a uniform distribution of Ni nanoparticles. The selected area diffraction pattern (SADP) obtained from TEM analysis of graphene showed typical hexagonal symmetry, which confirmed the crystallinity of graphene (Figure 5c). The average size of Ni nanoparticles (NPs) in the graphene–Ni structure was ≈ 25 nm (Figure 5d). In Raman spectra, the graphene synthesized without Ni nanoparticles had $I_D/I_G > 1$ (Figure 5e), but graphene synthesized with Ni nanoparticles had $I_D/I_G < 1$; the reason is that Ni has a catalytic function. The removal of oxygen-containing impurities by Ni could yield high-quality graphene. In the presence of Ni nanoparticles, exfoliation increased as the annealing temperature was raised from 1000 to 1600 °C. As a result, I_D/I_G tended to decrease, and the 2D peak was larger than the D peak (Figure 5f). At 1600 °C, I_D/I_G was 0.37 and I_{2D}/I_D was 4.25. The minimum temperature for graphene formation in the absence of Ni nanoparticles was 1200 °C, but exfoliation was incomplete, so the 2D peak was smaller than the D and G peaks. At temperatures higher than 1400 °C, graphene fragmented, so the I_D/I_G value increased. The present method was considered to be environmentally friendly, because it uses low-cost natural materials as carbon sources, and does not use harmful substances.

Graphene can also be synthesized from sugars.^[37] In this study, a sugar solution was mixed with sand and dried,

carbonized at 200 °C, and then annealed by rapid heating to 750 °C. These process converted sugar solution to graphene–sand composite (GSC) (Figure 6a). In Raman spectra (Figure 6b) of the composite loaded with 1 wt% GSC, the intensities of the D and G bands increased as carbonization temperature increases (250–750 °C); this change suggests that the graphitization of graphenic material increased with increase in temperatures. The X-ray photoelectron spectroscopy (XPS) spectrum of the GSC has peaks of all expected elements such as silicon, carbon, and oxygen (Figure 6c). An SEM image shows thin protruding sheets of carbon with nanometer thickness (Figure 6d). A TEM image taken after sonicating GSC also shows nanometer-sized thin sheets with a few wrinkles at the edges, like any graphene-like materials (Figure 6e).^[64] As a practical application of GSC, it was used in water purification; rhodamine 6G (R6G) (Figure 6f) and cola (Figure 6g) were filtered separately using different columns filled with GSC. The clear liquid after filtration indicated a complete removal. Analysis of the R6G liquid after filtration confirmed that it had been removed. The adsorption capacity was determined using R6G model dye and Chlorpyrifos insecticide. The capacity of GSC was 50–55 mg g⁻¹, which is higher than the maximum capacity of activated carbon under optimal conditions. Accordingly, the graphene synthesized by this inexpensive and ecologically friendly pyrolysis of sugar could be used as a recyclable commercial filtering agent and to purify drinking water.

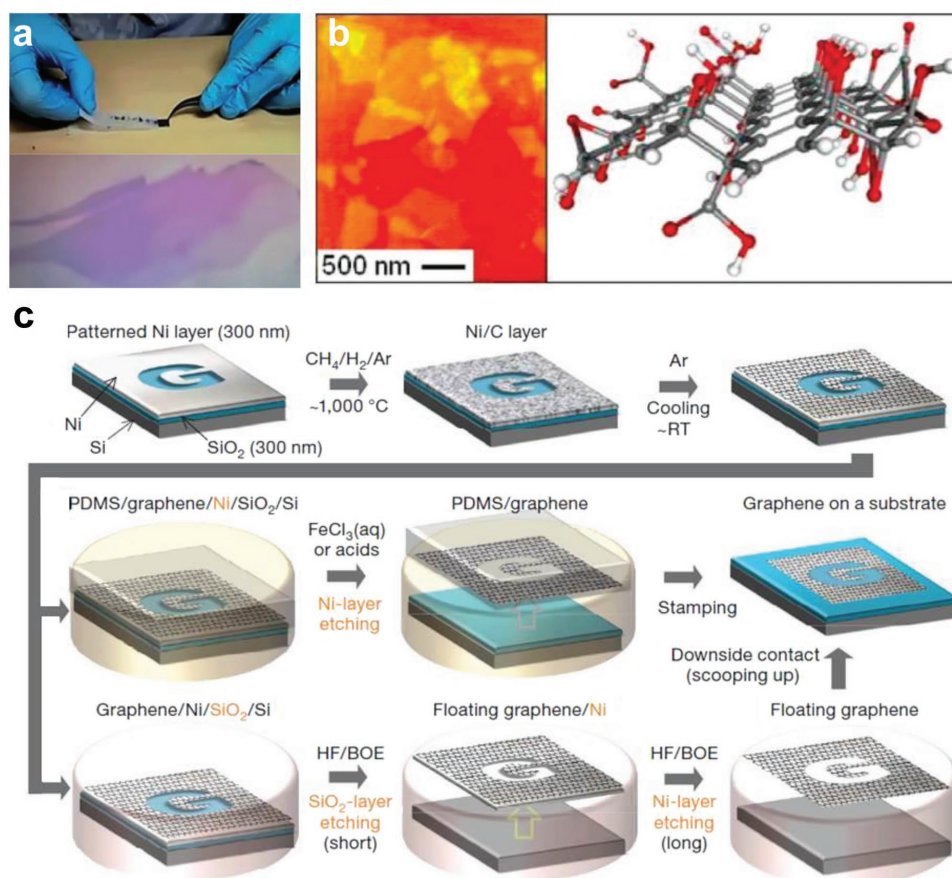


Figure 3. Conventional methods to synthesize graphene. a) Mechanical exfoliation using scotch tape (top), and transferred graphene using the same methods (bottom). Reproduced with permission.^[48] Copyright 2015, Royal Society of Chemistry. b) AFM image (left), and molecular structure of graphite oxide. Reproduced with permission.^[50] Copyright 2007, American Chemical Society. c) Schematics of CVD growth and transfer process of graphene. Reproduced with permission.^[52] Copyright 2009, Nature Publishing Group.

Table 1. Graphene synthesis by various methods, carbon sources, products, characteristics, and their applications.

Process	Carbon source	Product	Catalyst	Characteristics	Application	Ref.
Pyrolysis	Leaves	Few-layered graphene solution	–	–	–	[36]
Pyrolysis	Petal	Graphene or Ni-decorated graphene	Ni	–	–	[53]
Pyrolysis	Sugar	Graphene–sand composite	–	–	Water purification	[37]
Pyrolysis	Asphalt	Graphene–sand composite	–	–	Water purification	[54]
Pyrolysis	Sugar and urea	n-Doped graphene	–	–	Catalyst of oxygen reduction reaction	[35]
CVD	Cookies, roaches, dog feces, etc.	Single-layered graphene	Cu foil	$T = 97.3\% @ 550 \text{ nm}$	–	[55]
CVD	Plastic	Graphene films	Cu foil	–	–	[34]
CVD	Raw coal	Few-layered graphene	Cu foil	$5000 \Omega \text{ sq}^{-1}$, $T = 95\%$	–	[56]
CVD	PMMA, PS, PAN	Few-layered graphene	Ni	–	–	[57]
CVD	Coal tar pitch	Few-layered graphene	Ni	$1000 \Omega \text{ sq}^{-1}$	OFETs	[33]
CVD	PDMS	Graphene/dielectric	Ni	–	OFETs	[58]
Plasma	Honey, sugar, butter, milk, etc.	Vertical graphene	–	–	Biosensing or bioimmobilization	[59]
Plasma	Raw coal	Graphene–noble metal composite sheet	Pt, Ru, PtRu particles	–	Catalyst	[60]

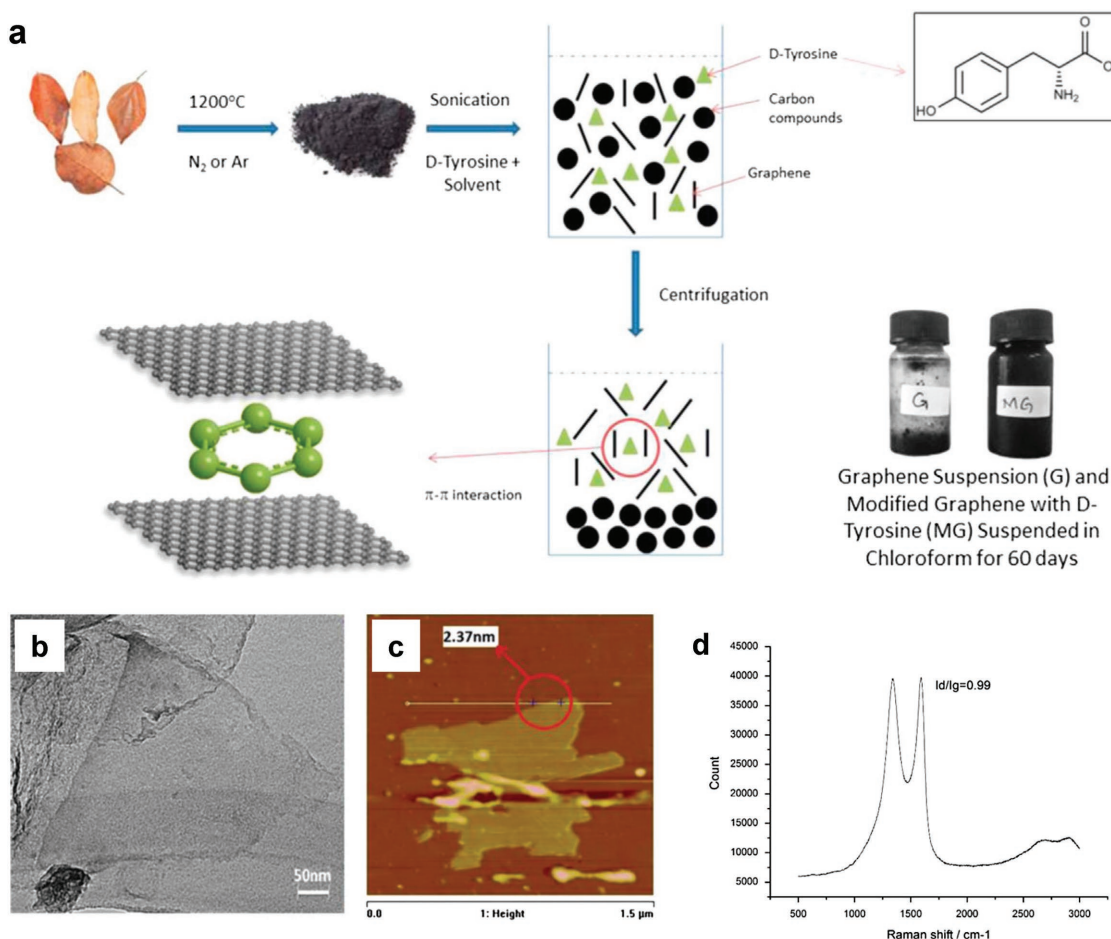


Figure 4. a) Schematic drawings of graphene synthesis, b) HR-TEM, and c) AFM images and d) Raman spectra of graphene obtained from leaves. Reproduced with permission.^[36] Copyright 2015, Elsevier.

In the same way, GSC was synthesized using asphalt, instead of sugars, for water purification applications (Figure 7a).^[54] GSC obtained using asphalt (GSC_{ASP}) was characterized by using microscopic techniques. The SEM images show sheet-like structure covering the surface of the sand (Figure 7b,c). Electron dispersive spectroscopy (EDAX) (Figure 7d) revealed that major elements present are carbon, silicon, and oxygen. The large carbon feature suggests that graphenic material formed over the sand. Since the rate of absorption is a very important factor in batch design and absorption process control, a test of pollutant removal test over time was conducted (Figure 7e). R6G was used as the model pollutant (10 mL) and 500 mg of 1 wt% GSC_{ASP} was used as an adsorbent. Over 65% of the R6G was removed in the first 60 min, and a pseudoequilibrium was reached after 240 min. Ho and McKay's pseudosecond-order kinetic model described the absorption result well.^[65,66] Prepared GSCs were used in practical applications (purification) to adsorb R6G from water. In batch experiments, RGO@RS^[67] had the adsorption capacity $q = 60 \text{ mg g}^{-1}$, GSC₇₅₀^[37] had $50 \leq q \leq 55 \text{ mg g}^{-1}$, and GSC_{ASP} had $q = 75.4 \text{ mg g}^{-1}$. In fixed-bed experiments, RGO@RS had 48 times higher q than regular sand, and GSC_{ASP} had 60 times higher q than regular sand (Figure 7f). These results

confirmed that graphene derived from inexpensive asphalt can be used in water purification.

Graphene prepared by pyrolysis methods exhibited limited quality (i.e., large D band and substantial impurities). Electrical and optical properties of graphene from pyrolysis of carbon waste have rarely been reported, but they would be poor because of the low quality of the synthesized graphene. Therefore, it is not suitable for use in optoelectronic application, where high electrical and optical properties are necessary. To be usable in optoelectronics, the quality of graphene derived from waste must be improved.

2.2.2. CVD

CVD is a well-known method to synthesize large-area graphene of high quality from gaseous sources on a catalytic substrate. This section discusses use of CVD to grow graphene from carbon wastes. Graphene has been achieved by using an inexpensive polymeric solid carbon source (e.g., polymethylmethacrylate (PMMA) and sucrose) instead of high-purity gaseous carbon precursors because the polymeric carbon source can be decomposed to gaseous precursors which react to form

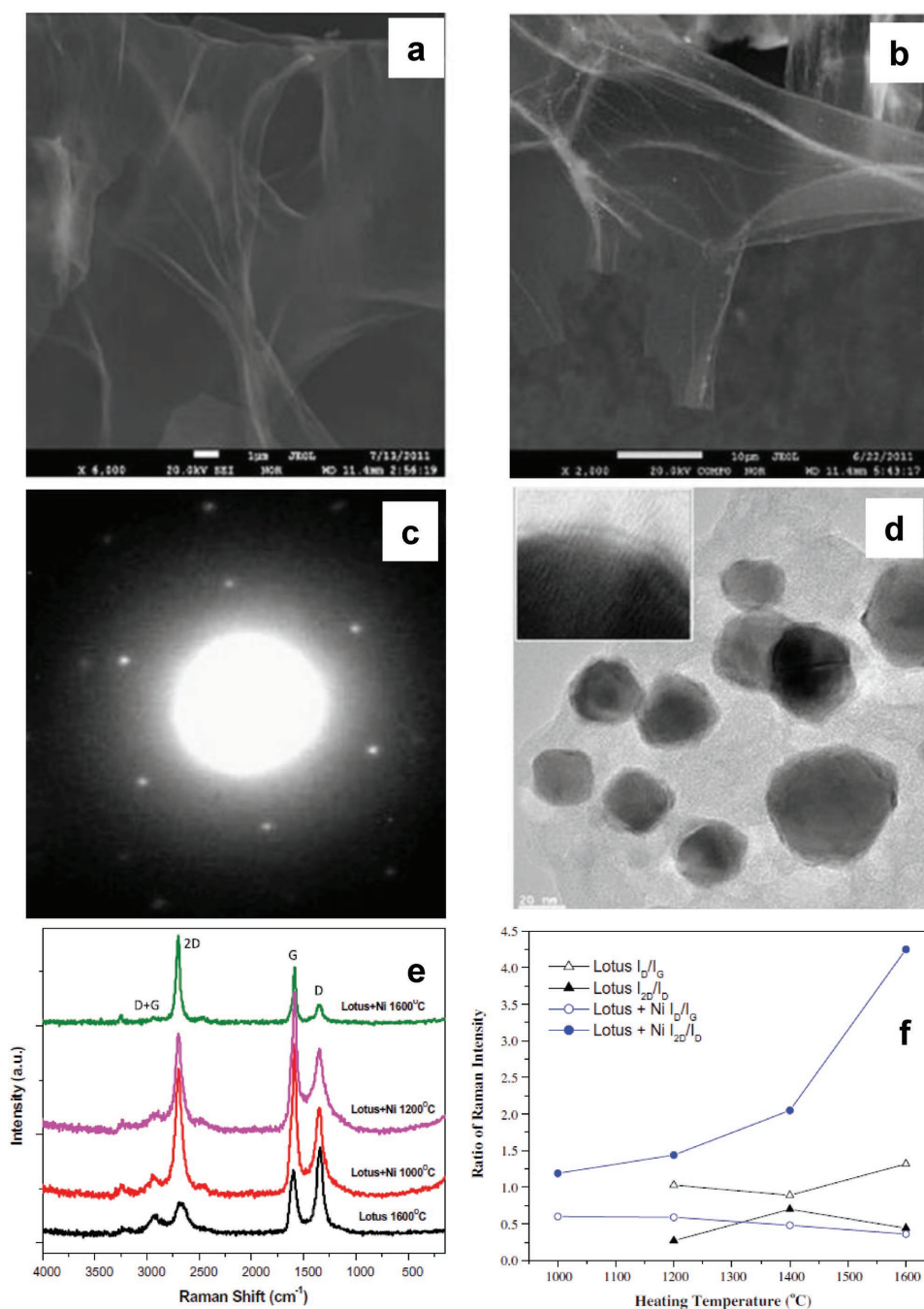


Figure 5. SEM image of a) graphene and b) graphene–Ni prepared from lotus flower petals at 1600 °C. c) TEM SADP of graphene. d) HR-TEM of graphene–Ni. Inset: Interface of graphene–Ni nanoparticle structure. e) Raman spectra of graphene and graphene–Ni synthesized at different temperatures. f) I_D/I_G and I_{2D}/I_D intensity ratios from Raman spectra of graphene prepared with and without Ni at different heating temperatures. Reproduced with permission.^[53] Copyright 2012, Elsevier.

graphene on a catalytic metal substrate above the decomposition temperature.^[63] Polymeric carbon precursor was spin-cast on Cu catalyst, then annealed at high temperature (>800 °C) under a reductive gas mixture (H_2/Ar) (Figure 8a). Graphene converted from PMMA showed a high I_{2D}/I_G value of >4, and clear 2D and G bands with negligible D band; these results indicate that the PMMA had been converted to high-quality single-layered graphene (Figure 8b). Electrical properties of the

PMMA-derived graphene were measured by using FETs which have PMMA-derived graphene as a channel (Figure 8c). FETs with PMMA-derived graphene had hole mobility $\approx 410 \text{ cm}^2 \text{ V}^{-1} \text{ s}^{-1}$, and on/off ratio ≈ 2 . Hexagonal structures in the SAED pattern (Figure 8d) and the TEM image (Figure 8e) indicated that PMMA had been converted to graphene. By controlling the flow of reductive gases (Ar or H_2), the number of layers in the graphene can be controlled. Converted single-layered graphene

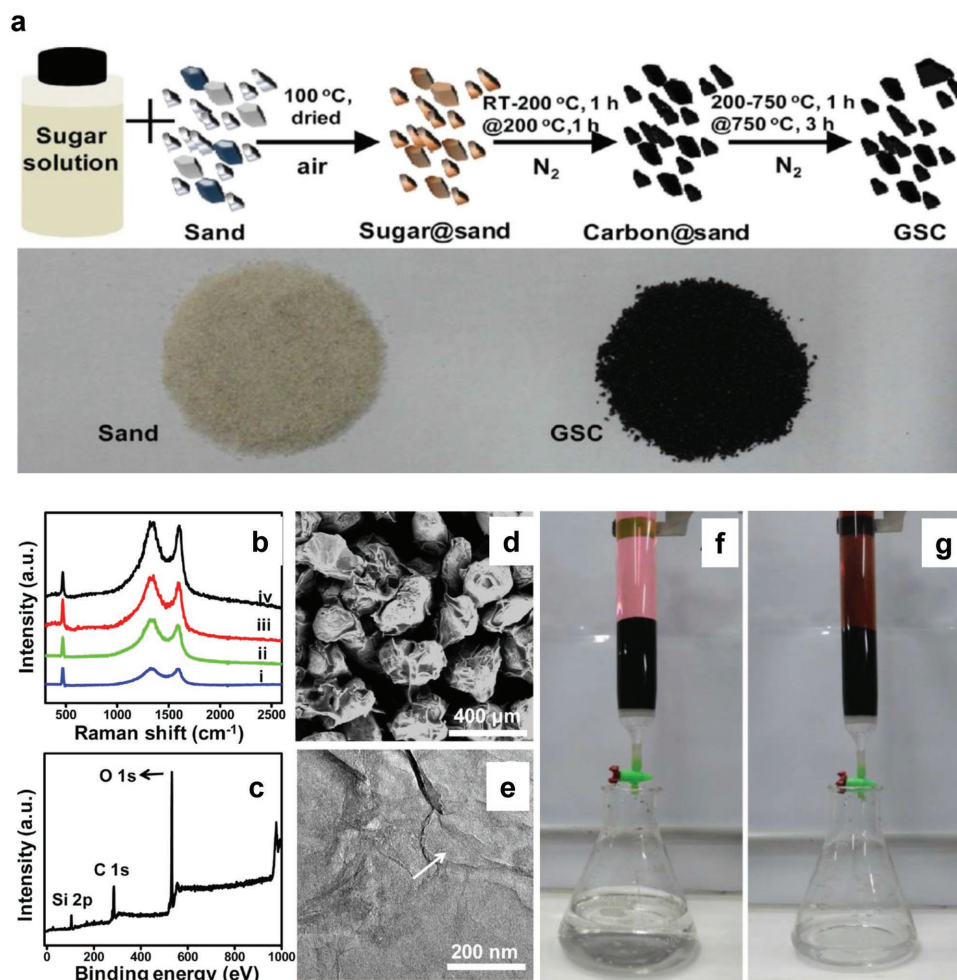


Figure 6. a) Schematic drawings of the preparation of graphene-sand composite (GSC) (top) and photographs of sand and GSC (bottom). b) Raman spectra of composites prepared at i) 250 °C in O₂ atmosphere, ii) 450 °C in N₂ atmosphere, iii) 600 °C in N₂ atmosphere, and iv) 750 °C in N₂ atmosphere. c) XPS spectrum of GSC. d) SEM images of GSC and e) TEM image of graphenic sheets with a few wrinkles. Photographs of adsorption columns using GSC to separate f) R6G and g) cola from aqueous solution. Reproduced with permission.^[37] Copyright 2012, American Chemical Society.

had OT = 97.1% at wavelength $\lambda = 550$ nm and sheet resistance $R_{sh} = 1200 \Omega \text{ sq}^{-1}$. Graphene with these characteristics is suitable for use as a transparent electrode in optoelectronics. To control the electrical properties of graphene derived from polymer, PMMA was mixed with hydrocarbon molecules that also contain N (melamine, C₃N₆H₆), then used to synthesize N-doped graphene from solid carbon precursors, by the same thermal and gas treatments used on pure PMMA (Figure 8f,g). The N-doped graphene had a strong D band, which is inevitable because the N heteroatom breaks the symmetry of the graphene, but electrical properties can be modified by single synthesis step (Figure 8h). A similar approach has been used to convert various polymers (polystyrene (PS), polyacrylonitrile, and PMMA) as carbon precursors in graphene synthesis.^[57] In each case, a polymer solution was spin-cast on the Si/SiO₂ substrate to form a 10 nm thick precursor layer, then a Ni capping layer was deposited on top of the precursor layer, and the assemblage was heated at ≈ 1000 °C in Ar/H₂ gas. This protocol converted polymeric precursors to graphene (Figure 9a). By

changing the thickness of the Ni layer, FLG with insignificant D band was synthesized (Figure 9b). High-resolution TEM (HR-TEM) image showed three to five layers of graphene (Figure 9c,d). These CVD approaches^[57,63] demonstrate the feasibility of using inexpensive carbon sources or carbon waste to synthesize high-quality graphene.

Various wastes such as cookies, chocolate, grass, plastics, roaches, and dog feces have been used as carbon sources for graphene synthesis. Each one was placed on a Cu foil and thermally annealed at 1050 °C under a H₂/Ar atmosphere.^[55] Monolayer graphene formed on the bottom of the Cu foil, and non-carbon components formed a residue on the top, i.e., high-value-added graphene could be achieved without purification (Figure 10a). The graphene that formed on the Cu foil was transferred to a target substrate by a conventional transfer method that uses PMMA. Raman spectra showed a small or negligible D peak, which indicates that the formed graphene has an insignificant degree of defects in its carbon lattice.^[61] Raman spectra had a large I_{2D}/I_G ratio, and OT $\approx 2.3\%$

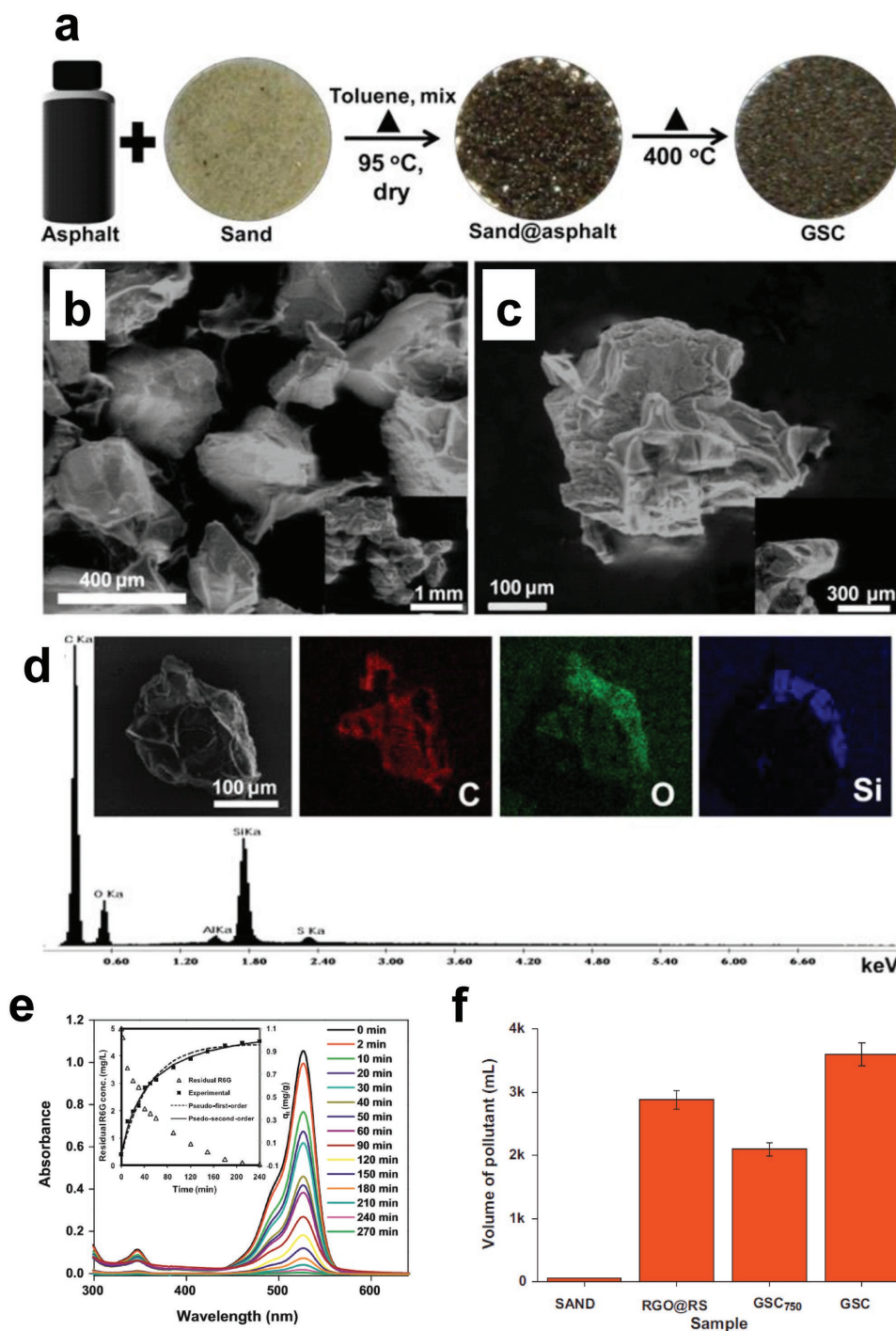


Figure 7. a) Schematic illustration of the formation of GSC. b,c) SEM images showing clustered particles and d) EDAX spectrum and corresponding elemental maps of GSC (5% loading). Insets in panels (b) and (c): corresponding asphalt-coated samples before heating. e) UV–vis data showing removal of R6G over time. Inset: removal of R6G versus time (primary axis), with pseudofirst- and pseudosecond-order model fits (secondary axis). Initial R6G concentration = 1 mg L^{−1}; flow rate = 2.3 mL min^{−1}. f) Adsorption capacity of different graphenic adsorbents (estimated error bar = ±5%). Reproduced with permission.^[54] Copyright 2013, Elsevier.

at $\lambda = 550$ nm (Figure 10b,c); these attributes confirm that the graphene is single layered.^[39,63] TEM detected a hexagonal diffraction pattern (Figure 10d), which confirmed that the crystallinity of the graphene and continuity of the graphene surface (Figure 10e). An edge image also showed a single layer

of graphene (Figure 10f). This study revealed the potential of using miscellaneous low-valued or negative-valued wastes without purification as high-quality graphene sources for use in optoelectronics, where it must have outstanding electrical and optical properties.

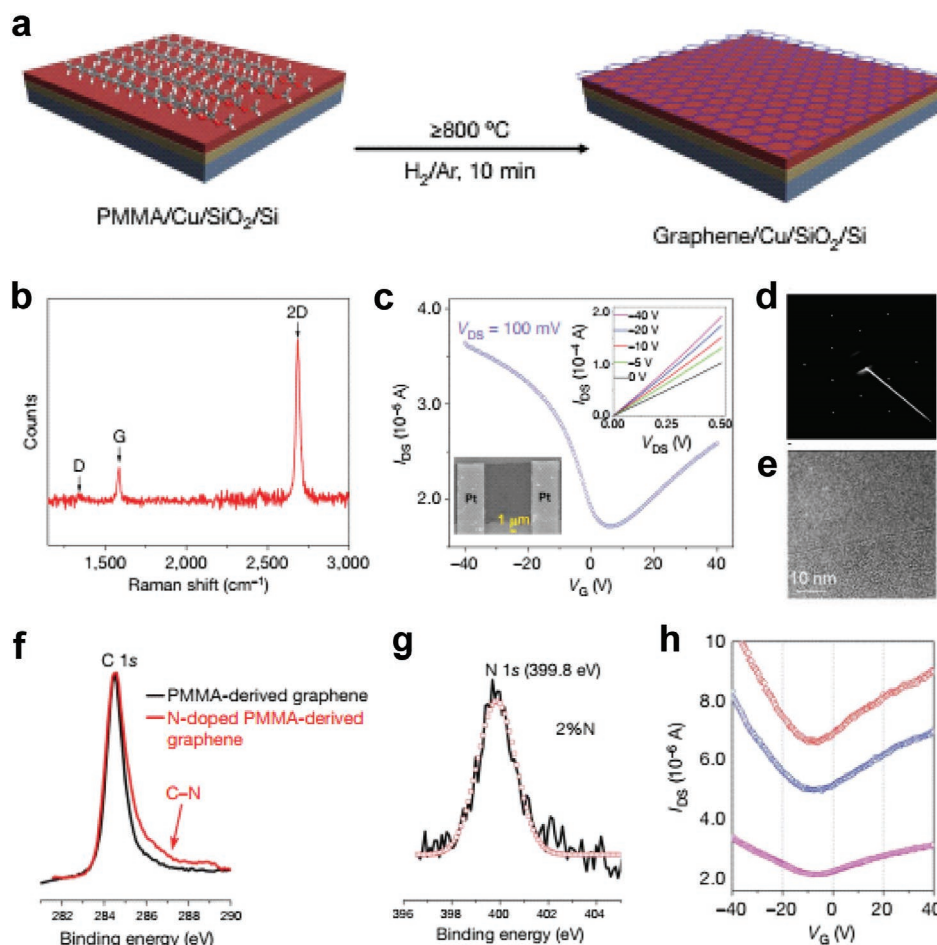


Figure 8. a) Schematic of method to produce PMMA-derived graphene and b) its Raman spectrum. c) I_{DS} versus V_G of PMMA-derived graphene FET (inset: I_{DS} vs V_{DS} at various V_G). d) SAED and e) HR-TEM images of PMMA-derived graphene. f) C 1s and g) N 1s in XPS of pristine and n-doped PMMA-derived graphene. h) I_{DS} versus V_G of three n-doped graphene FETs. Reproduced with permission.^[63] Copyright 2010, Nature Publishing Group.

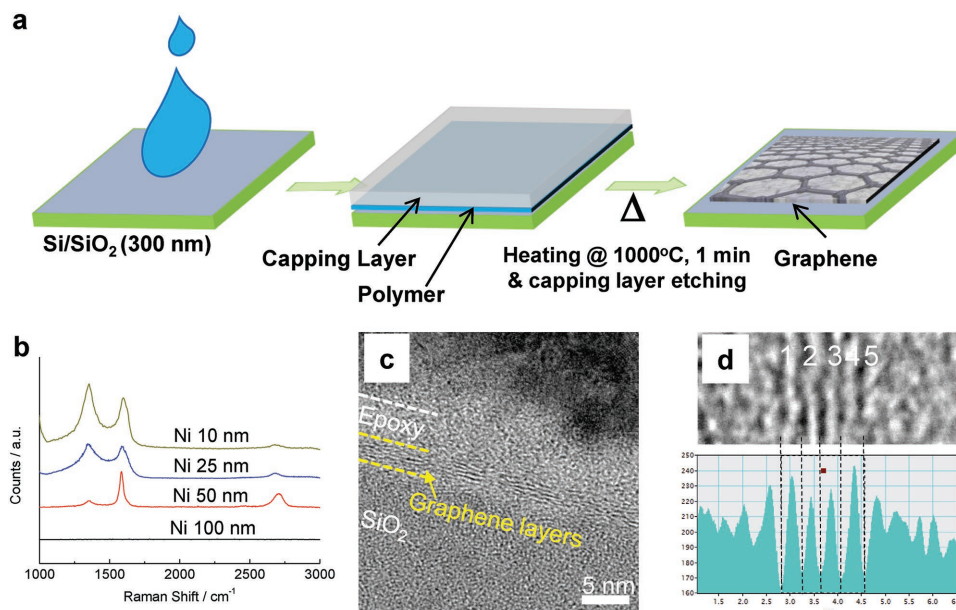


Figure 9. a) Schematics of graphene growth process. b) Raman spectra of graphene derived from polyacrylonitrile (PAN) at various Ni thickness. c) Cross-sectional and d) magnified HR-TEM image of polymer-derived graphene. Reproduced with permission.^[57] Copyright 2011, American Chemical Society.

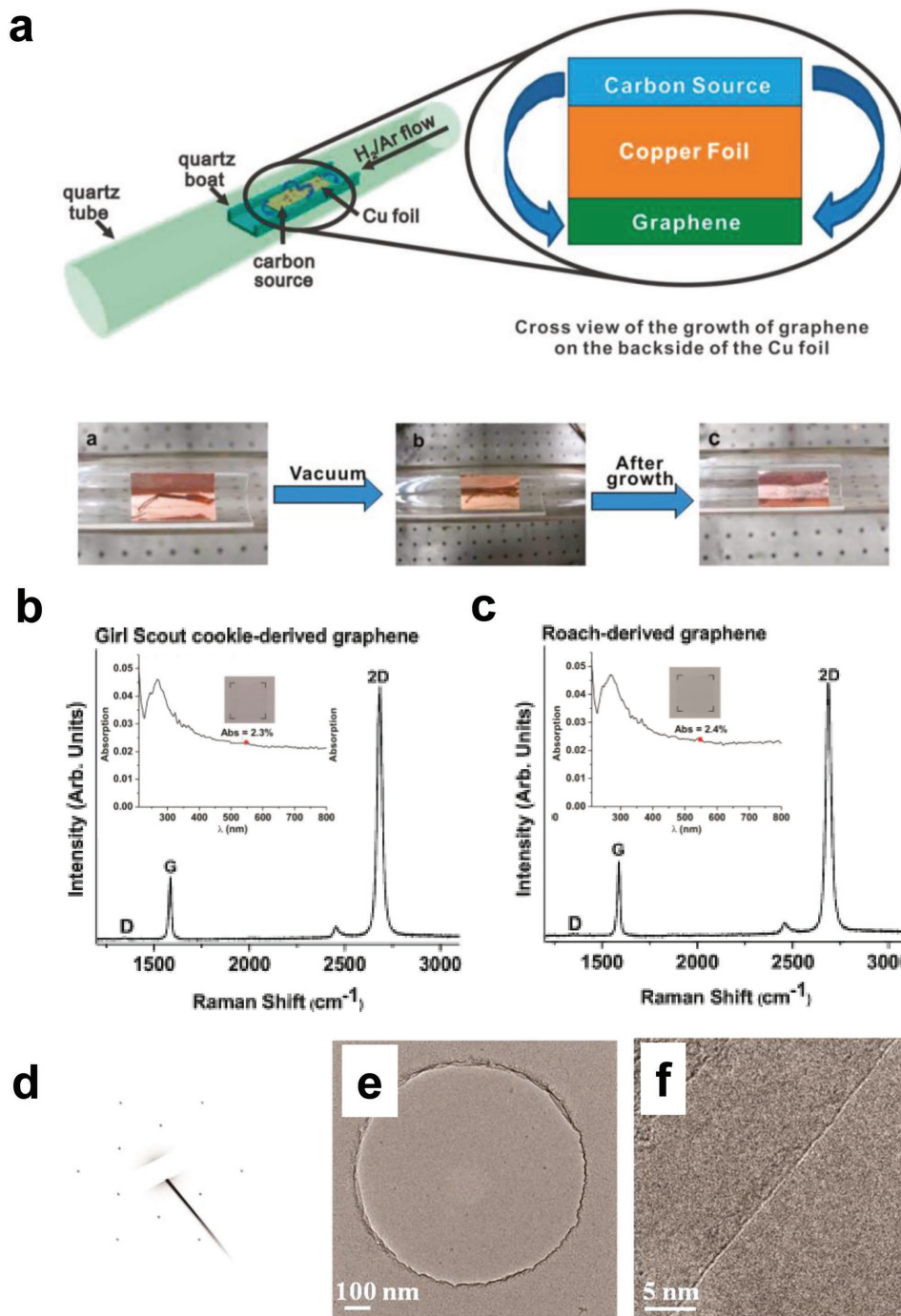


Figure 10. a) Schematic of experimental setup to synthesize graphene from inexpensive carbon sources with the Cu foil contained in a tube furnace (left), and cross-sectional diagram of formation of pristine graphene on the back side of the Cu substrate (right). Growth process is performed at 1050 °C under low pressure with a H₂/Ar gas flow. Raman spectra of graphene derived from b) cookie and c) roach (inset: optical transmittance). Diffraction pattern and TEM images of graphene derived from a cookie: d) SAED pattern, e) suspended graphene film on a 1 μ m diameter hole, and f) the edge of monolayer graphene. Reproduced with permission.^[155] Copyright 2011, American Chemical Society.

Graphene has been synthesized using waste plastics as raw materials.^[34] The main components of waste plastics polymers were polyethylene (86%) and polystyrene (14%). An ambient-pressure CVD method was used to convert precursor to graphene on a Cu foil (**Figure 11a**). The waste (**Figure 11b**) and Cu foil were each placed in a different furnace, and each was

annealed at different temperatures. As a result, single-crystal graphene formed. The growth rate of each single crystal was closely related to the rate of increase in pyrolysis temperature (ΔT_p) at which decomposed polymeric components from waste plastics were injected during pyrolysis. The study optimized ΔT_p as 1.5 °C min⁻¹. At $\Delta T_p < 1.5$ °C min⁻¹, the crystal size

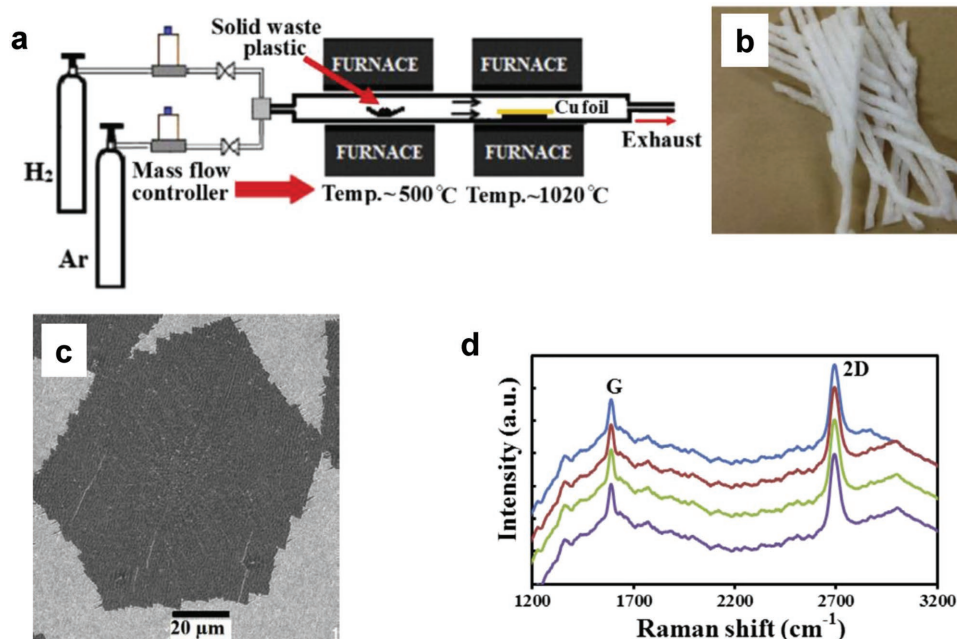


Figure 11. a) Schematic of the CVD process. b) Photograph of waste plastic used for graphene synthesis. c) SEM image of a graphene crystal. d) Raman spectra of the graphene crystal at randomly selected four different points. Reproduced with permission.^[34] Copyright 2014, Elsevier.

decreased due to insufficient injection of carbon atoms, but at $\Delta T_p > 1.5 \text{ } ^\circ\text{C min}^{-1}$, bi- and few-layered graphene are formed. To achieve large graphene crystals, nucleation density must be low. In this study, carbon radical flow was suppressed by decreasing the pyrolysis rate of waste plastics, so that graphene crystals of $\approx 100 \text{ }\mu\text{m}$ size could be obtained by continuous growth for 90 min (Figure 11c). Raman spectra of graphene crystal had a very small D band, which confirms the formation of very high quality graphene (Figure 11d). The spectrum showed a G band at 1590 cm^{-1} and a 2D band at 2700 cm^{-1} , with $I_G/I_{2D} < 1$, which confirmed the formation of single-layered graphene. The full-width half maximum (FWHM) values of the G and 2D bands were 19 and 44.2 cm^{-1} , respectively, which are consistent with those of single-layered graphene generated in a different report.^[55,68,69] Waste plastics could be used as raw materials to obtain controllable number of graphene layers with high-value-added graphene by simply controlling the rates of precursor injection and of temperature increase.

Raw coal has also been used for graphene synthesis.^[56] To achieve a simple and inexpensive process, a metal catalyst was used. The coal raw material and Cu foil were placed on separate quartz boats and moved to the heating zone at the center of a vacuum furnace filled with H_2 (Figure 12a). The graphene was synthesized by annealing at $1050 \text{ } ^\circ\text{C}$, then transferred from the Cu foil to a flexible substrate (Figure 12b). The 2D peak, which could not be observed in the Raman spectrum of raw coal (curve 2), was detected in the Raman spectrum of the resulting graphene (curve 1) (Figure 12c); this change confirms the formation of graphene. The presence of a D band in the Raman spectrum of graphene (curve 2) indicated the presence of defects, which might be due to various nonhydrocarbon gases generated during coal pyrolysis. The coal-derived graphene had $I_G/I_{2D} = 1.33$ and the FWHM of the 2D band was $\approx 57 \text{ cm}^{-1}$; these quantities

correspond to few-layered graphene.^[70,71] The graphene film on the substrate had OT $> 95\%$ at $400 \leq \lambda \leq 900 \text{ nm}$ (Figure 12d). The graphene formed continuously on a silicon substrate (Figure 12e) to a thickness of 5 nm, which is consistent with the few-layered graphene detected by the Raman spectrum. The graphene had $R_{sh} = 5000 \text{ }\Omega \text{ sq}^{-1}$. This graphene synthesized using the inexpensive and abundantly available raw coal was suitable for use in electronic devices as a flexible transparent conductor.

Graphene was later synthesized using coal tar pitch (CTP), which is a by-product of the steel industry.^[33] This study offered important insights for graphene industries into the future by synthesizing high-value-added graphene from industrial waste by using an environmentally friendly approach. CTP was dissolved in an organic solvent to form a thin film on a silicon substrate (SiO_2/Si) by the solution process. A Ni catalyst layer was deposited on top of the CTP layer, then the assembly was thermally annealed at $1100 \text{ } ^\circ\text{C}$ (Figure 13a); graphene formed from the CTP that was located between the substrate and the Ni layer. Unlike conventional methods, a thin film of raw material was deposited on the upper surface of a target substrate to synthesize graphene directly on it, instead of placing the raw material on a Cu foil to form graphene separately by annealing in a furnace. This method has advantages, because multilayered graphene could be achieved from the substrate–raw material layer–Ni catalyst layer structure by annealing, and the graphene could be synthesized on a substrate without a transfer process by removing the Ni catalyst layer using a Ni etching solution. The synthesized graphene was determined by Raman spectroscopy to have a multilayered structure ranging from monolayer to few layers (Figure 13b), and the cross section was observed by TEM (Figure 13c,d). Prepared multilayered graphene had $R_{sh} \approx 1000 \text{ }\Omega \text{ sq}^{-1}$ with minimum $R_{sh} = 906 \text{ }\Omega \text{ sq}^{-1}$, which is a substantial improvement over the previously reported graphene

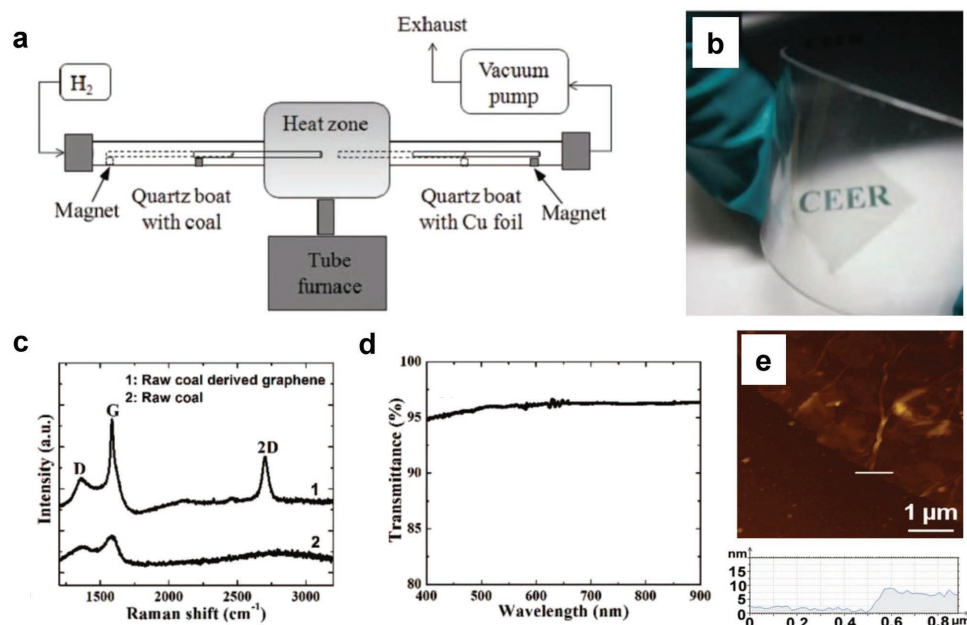


Figure 12. a) Schematic of the CVD setup: a quartz tube furnace connected to a vacuum pump and cylinder that contains pressurized H₂ gas. Magnets are attached to the two quartz boats used as support for the copper foil and coal. b) Photograph of graphene film on a flexible plastic substrate placed over the lettering "CEER." The size of graphene films is $\approx 1 \times 1$ cm². c) Raman spectra of raw coal (curve 2) and graphene film derived from it (curve 1). d) Optical transmittance spectrum of graphene film, which had OT > 95%. e) AFM image reveals continuous graphene film on silicon wafer; bright spots: wrinkles and overlaps. Reproduced with permission.^[56] Copyright 2013, Electrochemical Society.

obtained using carbon waste as a precursor. The synthesized graphene was applied as an organic field-effect transistor (OFET) electrode in a practical electronic device. Graphene-electrode pentacene FETs (Gr-P FETs) had even better electrical characteristics than the conventional Au electrode-based OTFT device (Au-P FETs) (Figure 13e). The contact resistance R_C of the graphene electrode was about two orders of magnitude lower than that of the Au electrode. This result occurs because the injection barrier from graphene to the pentacene channel is lower than the gold electrode, and in fact the Gr-P FET devices had higher field-effect mobility (maximum $\mu_{\text{FET}} \approx 0.36$ cm² V⁻¹ s⁻¹) than Au-P FETs (maximum $\mu_{\text{FET}} \approx 0.07$ cm² V⁻¹ s⁻¹) (Figure 13f).^[72,73] This technology allows simple solution process, so an OTFT device based on 144 graphene electrodes was fabricated on a 4 in. substrate to verify the possibility for scaleup. The large-area arrays showed $\approx 95\%$ of device operation (Figure 13g). Thus, this study provides the strongest evidence that graphene synthesized from carbon waste can be used in electronics.

Polydimethylsiloxane (PDMS) has also been used as an inexpensive carbon source.^[58] PDMS is solution-processable and can be used in dielectric layers.^[74,75] To substantially reduce the fabrication cost of electronic devices using graphene derived from a solid carbon source, bilayer structures composed of graphene layer with dielectric layer must be developed. If a thick-enough PDMS layer is deposited on Si layer, the PDMS can be used simultaneously as both a dielectric and a precursor of graphene time, because only interfacial region of PDMS underlying the catalyst is converted to the graphene. A Ni capping layer was deposited on PDMS, then thermal treatment yielded a PDMS/graphene/Ni/graphene structure (Figure 14a). At the interface between PDMS and

the underlying the Ni layer, carbon atoms diffused into the Ni catalyst at high temperature, and were released to form graphene on both sides of the catalyst layer. Raman spectrum mapping and their averaged spectrum of graphene grown in top and bottom of the Ni layer showed small I_D/I_G ratio (< 0.1 ; Figure 14b,c), which indicates that graphene grew on both sides of the Ni layer. By etching away the Ni layer, a substrate/dielectric/graphene structure was achieved without the need for transfer methods, which can damage the graphene. Graphene-pentacene organic FETs (GP-FETs) were fabricated by the deposition of a single channel layer of pentacene on this directly grown graphene electrode/dielectric layer without additional transfer process. This method, to fabricate GP-FETs, is simple compared to previous processes to fabricate OFETs that use graphene electrodes (Figure 14d). The transfer curve of the bottom-contact GP-FETs (Figure 14e) showed typical p-type characteristics and had $\mu_{\text{FET}} \approx 0.01$ cm² V⁻¹ s⁻¹ in the saturation regime and high on/off current ratio = 1.1×10^4 at gate voltage $-80 \text{ V} \leq V_G \leq 30 \text{ V}$. The GP-FET had very small hysteresis and a low density of deep traps between the insulating layer and the channel interface, and is therefore suitable as a switching device. The output characteristic of the GP-FETs show a clear gating effect and Ohmic contact due to the low R_C and charge injection barrier of the graphene electrode and the pentacene channel (Figure 14f).^[33] This method uses only a solution process and heat treatment, and therefore demonstrates that the graphene-containing structure formed from simple and inexpensive materials can be used both in conventional electronic devices and in flexible electronic devices.

So far, various approaches, which convert various inexpensive carbon feedstocks to graphene, have been studied. Among them,

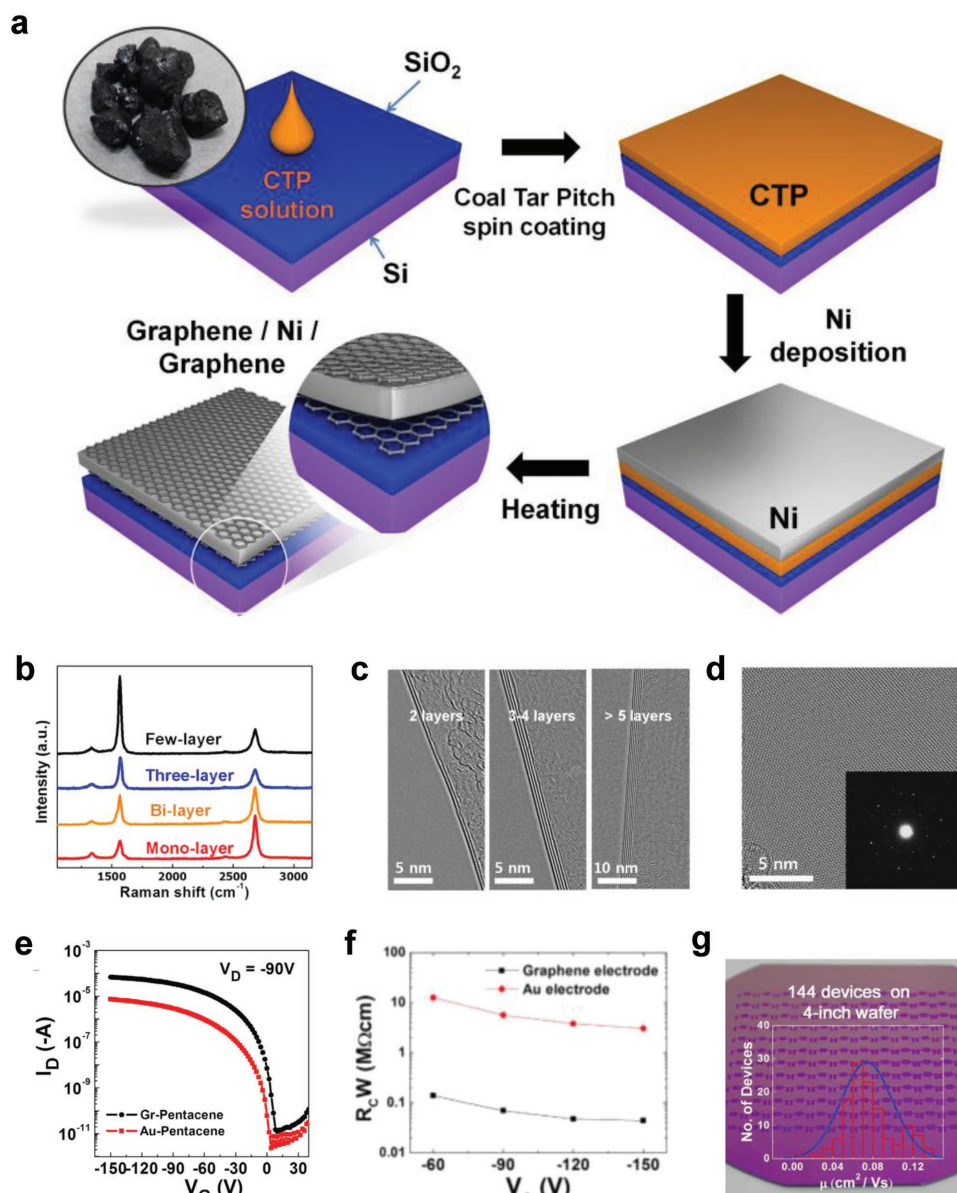


Figure 13. a) Schematics of basic procedure. b) Raman spectra of monolayer to few-layered graphene. c) TEM images of graphene films at the folded edge and d) surface (inset: electron diffraction pattern of graphene). e) Transfer curves of graphene-electrode pentacene and Au-electrode pentacene FETs (channel length: 100 μm). f) Contact resistances R_C of graphene and Au electrodes. g) Photograph of large-area Gr-P FET array (inset: histogram of the field-effect mobility μ_{FET}). Reproduced with permission.^[33] Copyright 2015, Nature Publishing Group.

catalytic pyrolysis and CVD showed best quality, which accompanied superior electrical properties. Previous recycling studies mostly confined to the high-quality synthesis itself. For the practical use of graphene derived from inexpensive carbon feedstocks, modification of graphene's electrical properties should be performed as well as synthesis of high-quality graphene. By employing carbon waste, which contains heteroatoms (e.g., B and N) on graphene synthesis, substantially doped graphene can be obtained. These chemical doping substantially modulates the electronic properties. Previously, C₃N₆H₆ was additionally mixed as an inexpensive N precursor.^[63] However, stoichiometric studies of substitutional doping from carbon wastes and direct substitutional doping research using carbon wastes that

intrinsically has heteroatoms have not been done in depth yet. Further attempts related to direct synthesis of substitutionally doped graphene from carbon waste would be also important for facile modification of graphene's electrical properties with the advantages of inexpensive and safe process; so it can broaden the electronic uses of graphene derived from carbon waste.

2.2.3. Plasma Treatment

As previously described, the synthesis methods of graphene from natural or industrial resources are environmentally friendly, resulting in high-value-added products. However, the

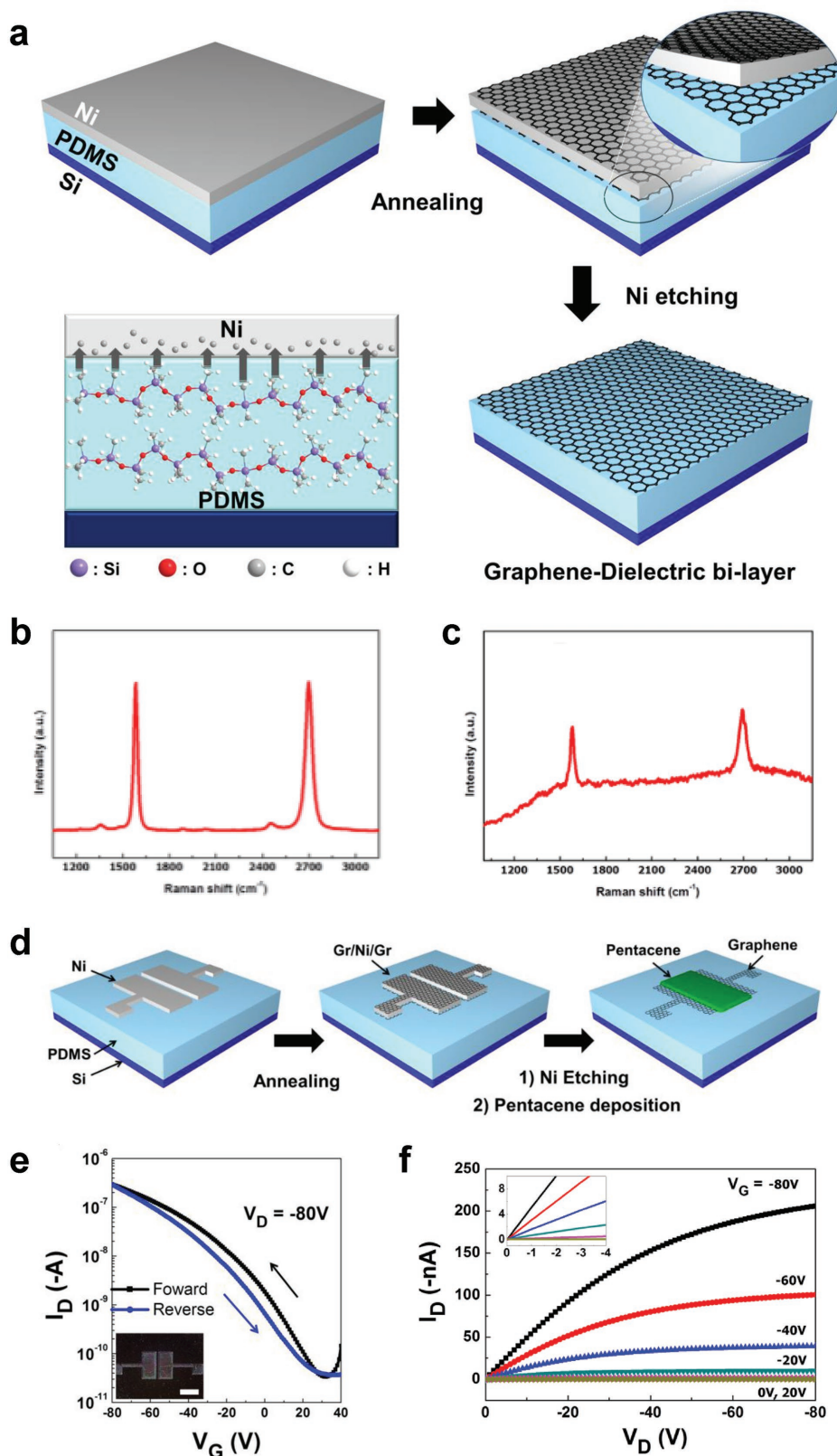


Figure 14. a) Schematics of procedure to synthesize graphene-dielectric bilayer structure. Raman spectrum of multilayered graphene grown b) on Ni layer and c) under Ni layer. d) Process to fabricate bottom-contact pentacene FETs based on graphene-dielectric bi-layer structure (GP-FETs). e) Transfer curves of GP-FETs, and f) output curves of GP-FETs (inset: output curves at low source-drain voltage). Reproduced with permission.^[58] Copyrights 2017, IOP Publishing.

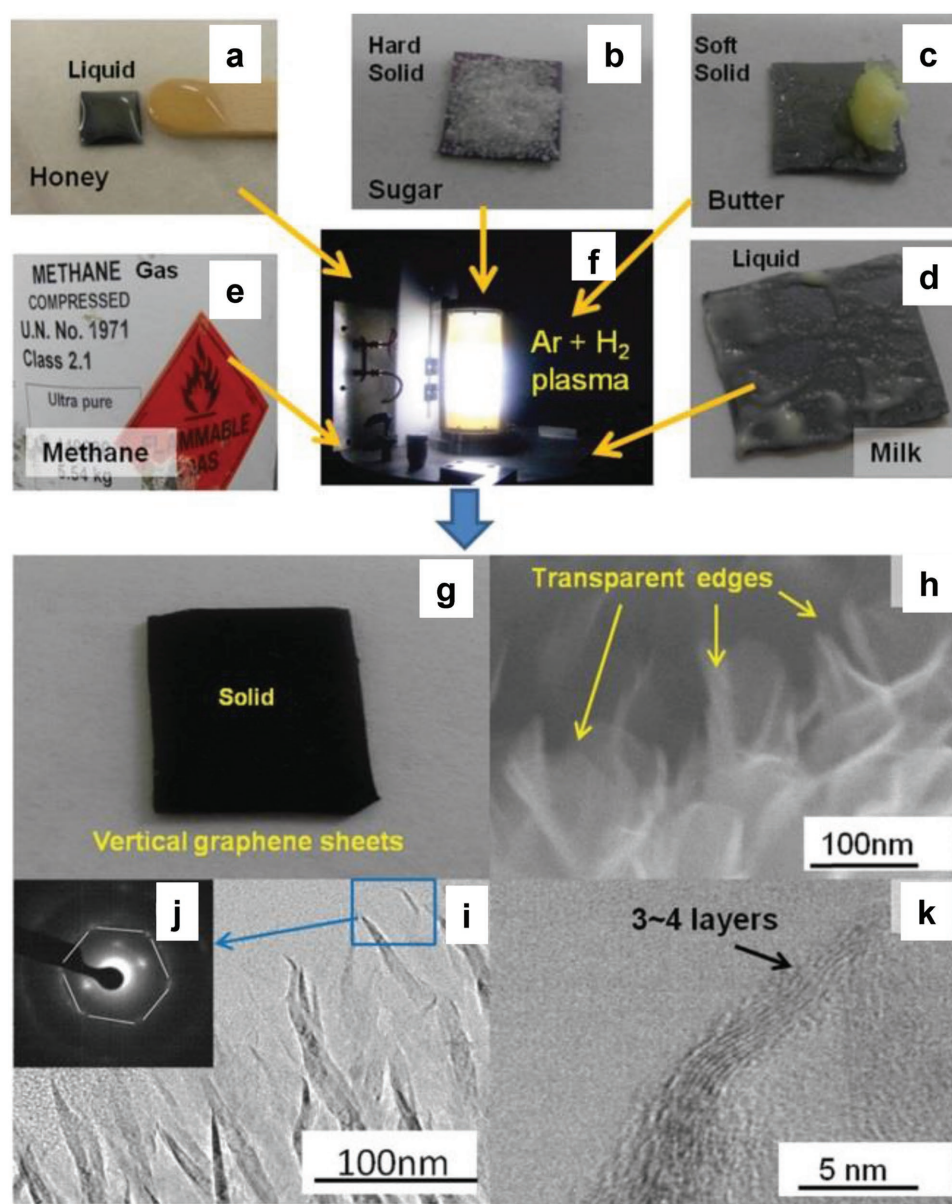


Figure 15. a–e) Preparation of vertical graphene (VG) from carbon precursors of various physical phases. Photographs of natural precursors in different states, pasted on clean SiO₂ substrates and f) the plasma used to produce VG. g) Photograph of VG sample obtained from honey after plasma process. h) Edges of MI–VGs transparent to the electron beam. i) TEM image of VGs and j) SAED pattern taken at the reactive edge of the VGs produced from honey. k) TEM image at the edge of VGs produced from butter. Reproduced with permission.^[59] Copyright 2013, Wiley-VCH.

processes are often complicated, precursor-specific, or require long durations in high-temperature conditions. A plasma process can yield carbon products simply at low temperatures without a catalyst.^[59] Synthesis mechanism of graphene using plasma treatment is described in previous reports.^[76,77] Vertical graphene (VG) has ultralong reactive edges and other unique characteristics, and therefore may have various applications in energy, electronics, environmental, and biological devices. VG nanosheets can self-organize to form a 3D-internetworked array structure, which has shown great potential as a component of functional devices, such as biosensors and supercapacitors.^[78,79] VG with uniform functional structure and excellent adhesion to a substrate was synthesized by using the plasma technique from

various gaseous, liquid, solid precursors with various chemical structures (e.g., honey, milk, methane, butter, and table sugar). This method has the advantage of being a simple single-step process that can be performed at low temperature with no catalyst. Plasma processing in Ar/H₂ mix was used to synthesize VGs from a) honey (HO), a viscous liquid; b) table sugar (TS), a crystalline (hard) solid; c) butter (BU), a soft solid; d) condensed milk (MI), a liquid; and e) methane (ME), a gas (Figure 15a–f). After the plasma process, VG had a typical black soot-like appearance (Figure 15g); it was transparent to an electron beam (Figure 15h), had a typical array structure (Figure 15i), and the VGs had about 3–4 layers (Figure 15k) with distinct hexagonal atomic arrangements. The functionality of the resulting VGs was investigated

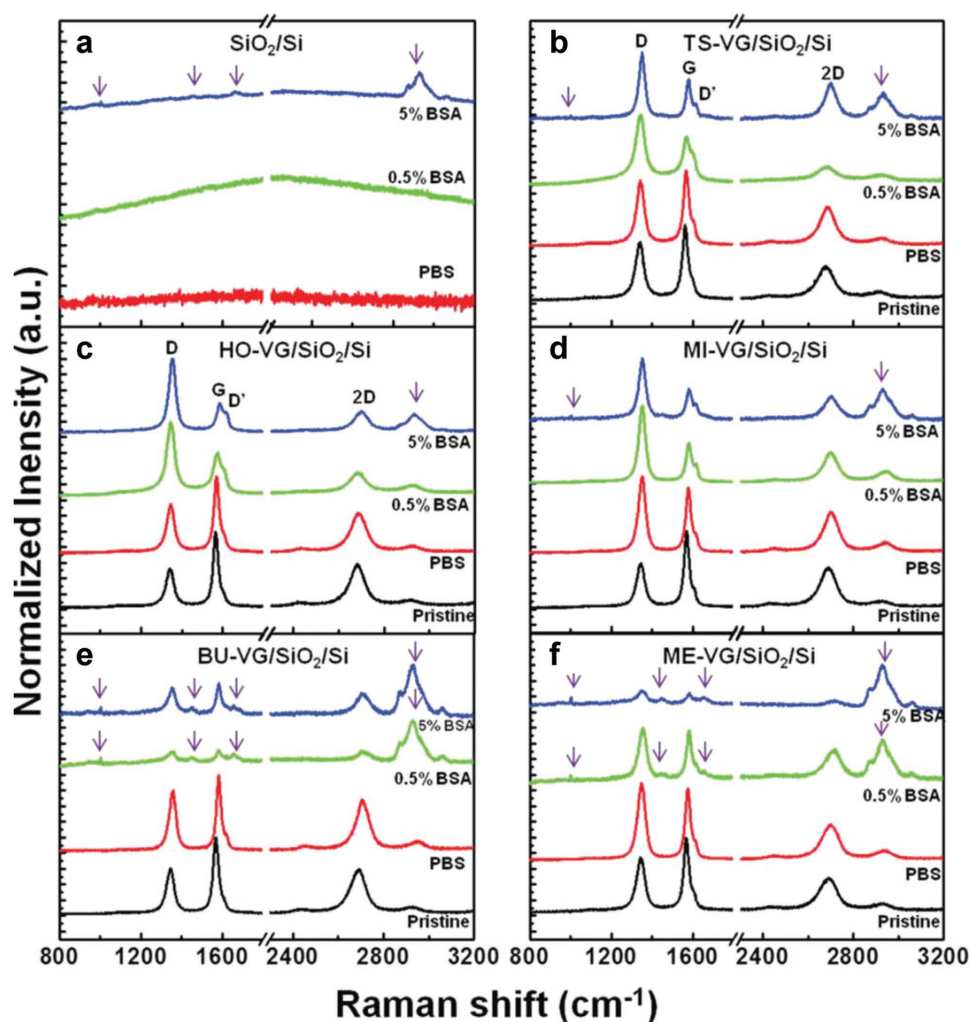


Figure 16. Responses of vertical graphene (VG) to biologically relevant chemicals. Raman spectra of PBS (red), 0.5% BSA (green), and 5% BSA (blue) on a) SiO_2 substrate, b) TS-VG/ SiO_2/Si , c) HO-VG/ SiO_2/Si , d) MI-VG/ SiO_2/Si , e) BU-VG/ SiO_2/Si , and f) ME-VG/ SiO_2/Si ; black spectra: pristine VG (arrows: Raman fingerprints associated with BSA). Reproduced with permission.^[59] Copyright 2013, Wiley-VCH.

by analyzing their effects on biologically relevant chemicals. VGs synthesized from different materials were treated with 5% or 0.5% (w/v) bovine serum albumin (BSA) in phosphate buffer saline (PBS), and characterized by Raman spectra. VGs synthesized from BU and ME had the highest reactivity for biosensing or bioimmobilization applications (Figure 16). The synthesis of functional nanostructures using plasma at a low temperature of 450 °C is an environmentally benign and an energy-efficient method that can use many types of organic precursor, and does not require external heat treatment or catalysts.

Graphene and graphene-noble metal composites have also been synthesized using plasma techniques and coal as the raw material.^[60] The graphene was synthesized by catalytic graphitization, chemical oxidation, and dielectric barrier discharge (DBD) plasma-assisted deoxygenation. GO was formed by acid treatment and graphitization of raw coal, whereas graphene sheets (GS) were produced using DBD plasma treatment. Taixi coal (TX) from Shanxi province, China, was used as the raw material to produce GS. To compare with the catalytically graphitized TX (TX-C-G), noncatalytically graphitized TX

(TX-NC-G) was oxidized using the Hummers method to obtain graphite-like carbon.^[49] Each one was then converted to GO (TX-C-GO, TX-NC-GO). Subsequently, GO was converted to GS by using the DBD plasma process (TXC-GS and TX-NC-GS) (Figure 17a,b). TX-NC-GS (Figure 17c–e) and TX-C-GS (Figure 17f–h) were observed using SEM and TEM. H_2 plasma reduction significantly decreased the number of oxygen-containing groups of TX-NC-GO and TX-C-GO (mainly C=O, C–O, and O–H) (Figure 17i). Raman spectra revealed significant structural changes in GS produced from coal-based graphite (Figure 17j). I_D/I_G was smaller in TX-C-G than in TX-NC-G; this difference means that TX-C-G was more strongly graphitized than TX-NC-G. The chemically derived graphene was applied as an electrode of a supercapacitor, and its characteristics were confirmed.^[78] In addition, NP/GS was synthesized using the same plasma reaction with noble metal (Pt, Ru, or PtRu) nanoparticles. The catalytic activity of NP/GS was determined by quantifying its selective reduction of NO_x . Results indicate that the graphene and graphene-based composites from coal could be applied to novel structures and various applications.

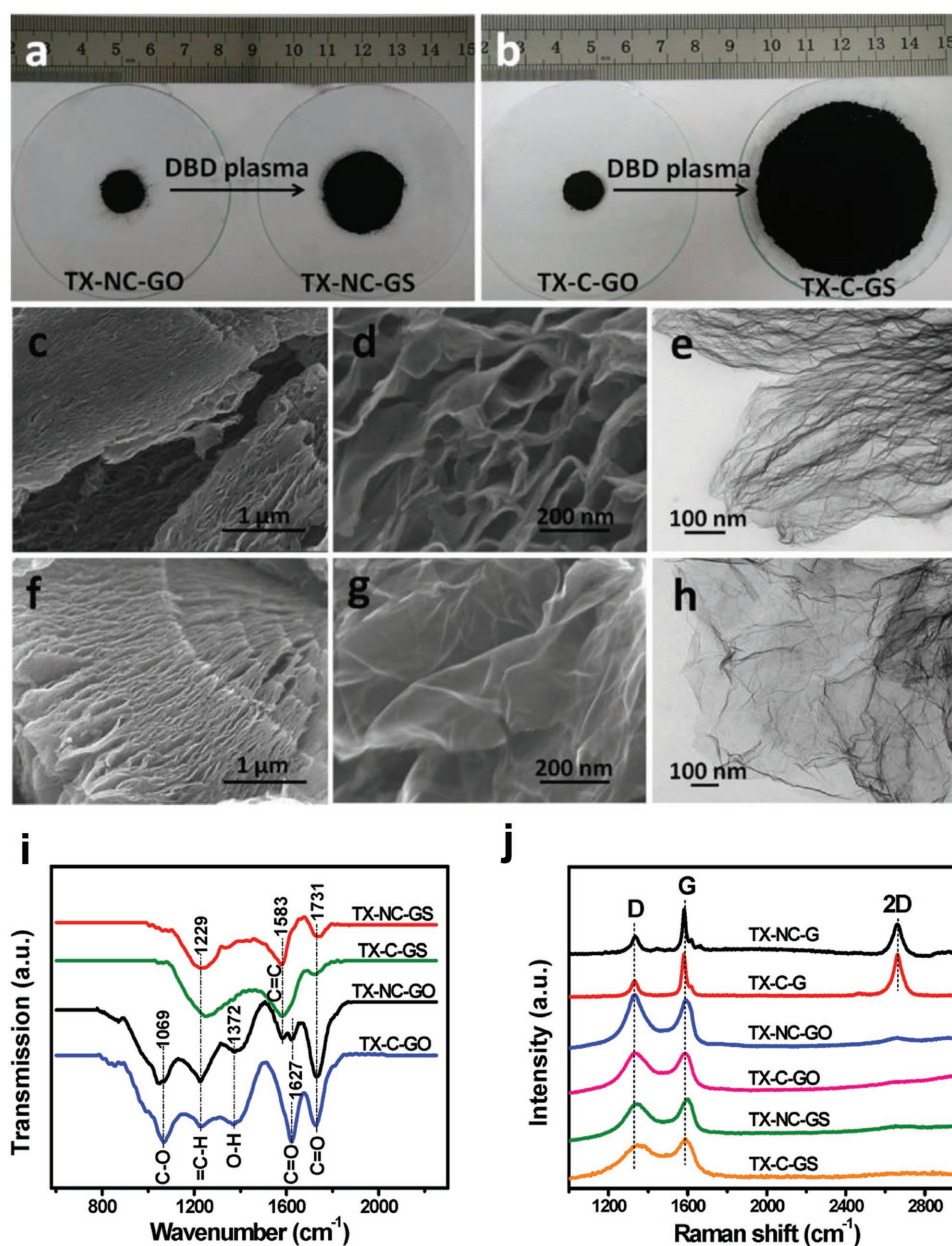


Figure 17. a,b) Photographs of samples before and after treatment. SEM and TEM images of c–e) TX-NC-GS and f–h) TX-C-GS at different magnifications. i) Fourier-transform infrared spectroscopy (FT-IR) results and j) Raman spectra of coal-based GO and GS. Reproduced with permission.^[60] Copyright 2012, American Chemical Society.

3. CNTs

3.1. Conventional Synthetic Methods for CNTs

An arc discharge is generated by applying DC bias between a graphitic anode and a graphitic cathode in a He-filled chamber. The anode contains carbon precursors for CNT synthesis, and the cathode is composed of a graphite rod (Figure 18a). The arc is high-temperature plasma (>4000 K), which sublimates the carbon precursors in the anode. The temperature gradient drives the vapors toward the cathode. After the arc is extinguished, CNTs are obtained from cathode. This method

has advantages of rapid production of CNTs with few defects; however, it has poor controllability and low productivity. To improve the productivity, optimization of fabrication conditions (e.g., type of inert gas, applied voltage, and rod size) has been attempted.^[80] Nevertheless, the productivity of the CNTs at the optimized condition is still far below the practical level, so alternative methods (e.g., laser ablation, CVD, plasma-enhanced CVD) have been developed.^[32,81]

Laser ablation prepares CNTs at high temperature (≈1200 °C). A target is composed of graphite with metal catalyst (e.g., Co and Ni); laser is applied to vaporize the carbon (Figure 18b). After a carbon-vapor atmosphere is formed, the chamber is

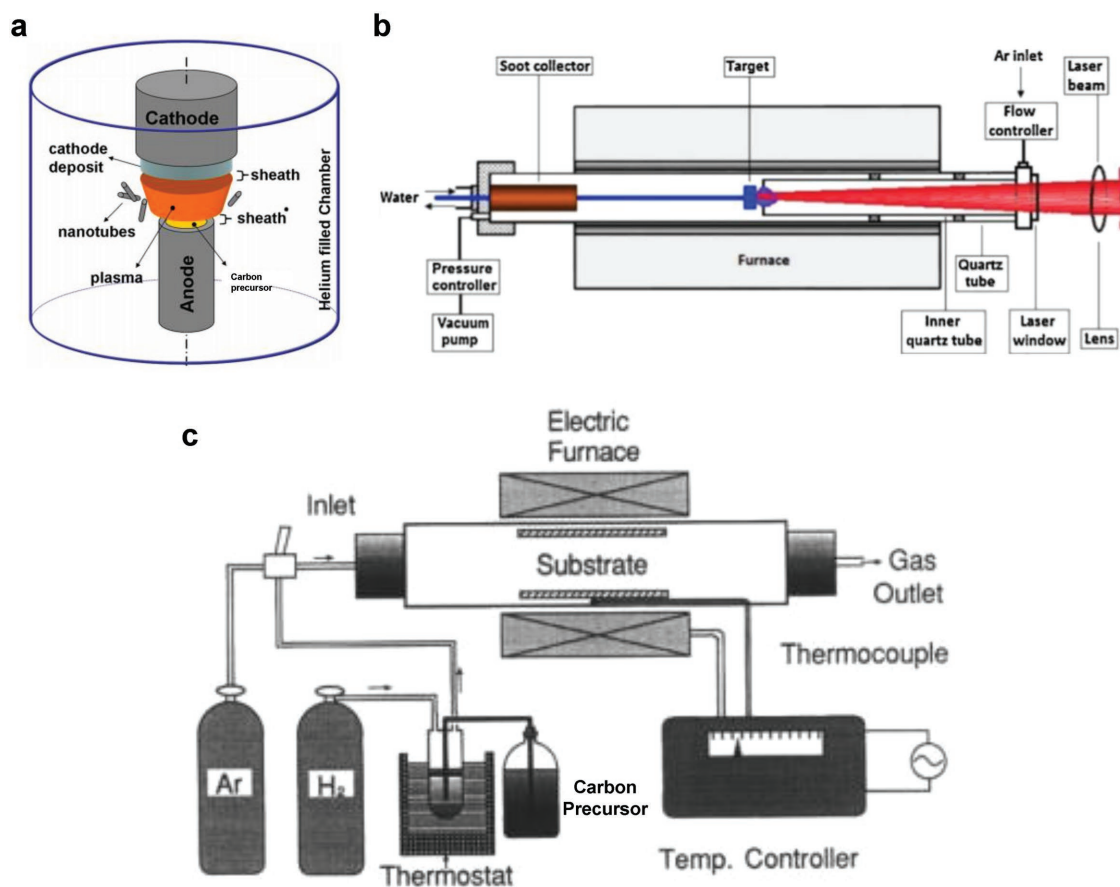


Figure 18. Schematics of conventional synthesis methods of CNTs. a) Arc discharge. Reproduced with permission.^[81] Copyright 2012, IOP Publishing. b) Laser ablation. Reproduced with permission.^[83] Copyright 2015, Wiley-VCH. c) CVD. Reproduced with permission.^[84] Copyright 1993, Elsevier.

rapidly cooled; the carbon in the vapor combines to form large molecules. Catalyst that is vaporized during the laser ablation prevents carbon particles from adsorbing to chamber structures.^[82] Combined carbon vapors can be collected on a water-cooled collector. Usually, CNTs synthesized by this method have higher purity than those produced by arc discharge, but productivity of CNT from laser ablation is low as well.^[83]

The CVD method has also been used to synthesize the CNTs. Among the various methods to synthesize CNTs, CVD is, currently, most widely used due to its low cost, high productivity, scalability, and easy controllability.^[84] The CVD process entails passing gaseous carbon precursors (e.g., CH_4 , C_2H_2 , and C_6H_6) through a CVD chamber, which holds a metallic catalyst (e.g., Fe, Co, and Ni) at high temperature (600–1200 °C) (Figure 18c). When carbon precursor vapors pass over the catalyst, they decompose into carbon and hydrogen. CNTs grow on metallic catalyst surface, and are collected after the CVD system is cooled.

The CNT growth mechanism is still being debated, but the generally accepted mechanism is as follows. Decomposed carbons dissolved into the metal catalyst. When the carbon concentration begins to exceed the solubility limit of the metal, dissolved carbons precipitate and crystallize to form a cylindrical network, which has no dangling bonds. Decomposition of the carbon precursor is an exothermic process; the released heat is transferred to the metal. Crystallization of carbon is an

endothermic process that absorbs heat from the metal. The process of decomposition and crystallization causes a thermal gradient that maintains CNT growth.

3.2. Synthesis of CNT Using Carbon Wastes

CNT synthesis from inexpensive carbon wastes was widely attempted. This section reports methods (Table 2) to synthesize CNTs from waste products and provides characteristics of the CNTs.

3.2.1. Pyrolysis

CNTs have been synthesized by pyrolysis of industrial carbon waste (i.e., printed circuit boards (PCBs)).^[85] Pyrolysis of the PCB was conducted at 600 °C in a reactor tube; the product was liquefied by passing it through a water condenser, and a liquid condenser (Figure 19a). This liquid was mixed and homogenized using ferrocene and ethanol, then thermally treated at 900 °C to yield CNTs that were several micrometers long, and were filled with metal particles and nanorods (Figure 19b,c). TEM refined the size measurements to a diameter of ≈ 338 nm and a thickness of ≈ 86 nm, and revealed a hollow structure

Table 2. Various methods to synthesize CNTs, with carbon sources, products, characteristics, and their applications.

Process	Carbon source	Catalyst	Product	Application	Ref.
Pyrolysis and catalytic growth	Printed circuit board	Ferrocene	Hollow-centered CNTs Outer diameter: ≈ 338 nm	–	[85]
Pyrolysis and catalytic growth	Polyethylene, polypropylene, polystyrene	Ni–Al	Multiwalled CNTs Diameter: 10–20 nm Length: several micrometers	–	[86]
Pyrolysis and catalytic growth	Polypropylene	Ni/Ca–Al and Ni/Zn–Al	Multiwalled CNTs Diameter: 50 nm Length: 10 μ m	–	[87]
Pyrolysis and catalytic growth	Plastic from a motor oil container, polyethylene, polyvinyl chloride	Ni–Mn–Al	Multiwalled CNTs Diameter: ≈ 30 nm (≈ 10 nm of wall thickness) Length: 1–10 μ m	–	[88]
Pyrolysis and catalytic growth	Waste glycerol	Ni–Al and Ni–Mg–Al	Multiwalled CNTs Diameter: 20 nm Length: 50 μ m	–	[89]
Pyrolysis and catalytic growth	Polyethylene	Cobalt acetate	Multiwalled CNTs Diameter: ≈ 80 nm Length: several micrometers Electrical conductivity: 43, 72 S m $^{-1}$	Water purification	[90]
Pyrolysis and catalytic growth	Polypropylene	Ni	Multiwalled CNTs Diameter: 10–25 nm $T = 85\%$ @ 550 nm	–	[91]
Pyrolysis and growth in nanoporous template	Plastic bag	–	CNT–nanoporous template membranes Wall thickness: 4–9 nm	Molecular separation membrane	[92]
Arc discharge	Polyethylene terephthalate	–	Multiwalled CNTs Diameter: 364 nm Length: several micrometers	–	[93]
Arc discharge	Fullerene waste soot	Ni and Y $_2$ O $_3$	Single-walled CNTs Diameter: 1.2–2.0 nm	–	[94]

(Figure 19d,e). X-ray diffraction (XRD) spectra showed sharp peaks at $\approx 25.9^\circ$ and $\approx 43.5^\circ$ (Figure 19f), which correspond to the (002) reflection of carbon and to the (100) plane, respectively; this result indicates the presence of sp^2 -hybridized carbons in a honeycomb lattice. Peaks of Fe ($\approx 44.70^\circ$, $\approx 50.83^\circ$) and Fe $_x$ C ($\approx 40.40^\circ$) were also observed. A CNT-formation mechanism can be suggested as follows: carbon species accumulate on the surface of nanometer-sized Fe that is produced by decomposition of ferrocene, and form Fe–C compounds. After reaching the saturation of carbon atoms on the surface of the Fe particle, C atoms nucleate, and self-organize to form CNTs.

Industrial plastic wastes (low-density polyethylene (LDPE), polypropylene (PP), and PS) have been converted to CNT using pyrolysis methods, in which steam is injected during the process (Figure 20a).^[86] Plastic waste was heated at 600 °C to gasify it, then additionally treated at 800 °C and passed through a Ni/Al $_2$ O $_3$ catalyst. The SEM image of the catalyst showed dense deposits of carbon filaments with lengths of several micrometers (Figure 20b). However, increasing the rate of steam injection causes oxidation of the carbonaceous species, so the yield of CNTs decreased. TEM image showed a large number of CNTs with diameter ≈ 10 nm (Figure 20c,d). Raman spectra showed G band (1589 cm $^{-1}$) and D band (1359 cm $^{-1}$), with $I_G/I_D > 1$, which means that the CNTs were of high purity (Figure 20e). Pyrolysis yields CNTs and H $_2$; the quantities have a trade-off relationship. To achieve high CNT yield, the steam rate must be

controlled carefully. CNTs and H $_2$ have been synthesized from plastic wastes by a similar method with Ni/Ca–Al and Ni/Zn–Al catalysts.^[87] Prepared CNTs were estimated to have a diameter of ≈ 50 nm and a length of ≈ 10 μ m (Figure 21a). The Raman spectrum of waste-derived CNTs had lower I_D/I_G and higher I_{2D}/I_G than did commercially available CNTs (Figure 21b); i.e., graphitization and purity were higher in waste-derived CNTs than in commercial CNTs.

CNTs have been obtained using polymer wastes (Figure 22a) and cobalt acetate (CoAc) catalyst (Figure 22b) at ≈ 700 °C; converted CNTs were tipped with nanometer-sized Co particles.^[90] Energy dispersive spectra and XRD results revealed that these CNTs consist of graphitic carbons with Co (Figure 22c). A growth mechanism of the CNTs was proposed (Figure 22d): polymer wastes dissociate at ≈ 700 °C to form a carbon mixture, CO $_2$, and various C $_x$ H $_y$. Catalytic behavior of CoAc yields the formation of carbon shells on metal particles. Edges of the graphite are chemisorbed onto the metal (Co), and the carbon species produced by dissociation of polymer wastes self-assemble on the surface of the Co. Additional carbon species can adhere to three places. At first, a graphite shell grows around the Co particle; this process covers and deactivates the Co catalyst. Second, additional shells form under the previous graphite shells, which are forced to form a cylindrical tube, of which the end is chemisorbed to the Co catalyst. Third, carbon species are added to the cylindrical carbon tubes. CNTs derived

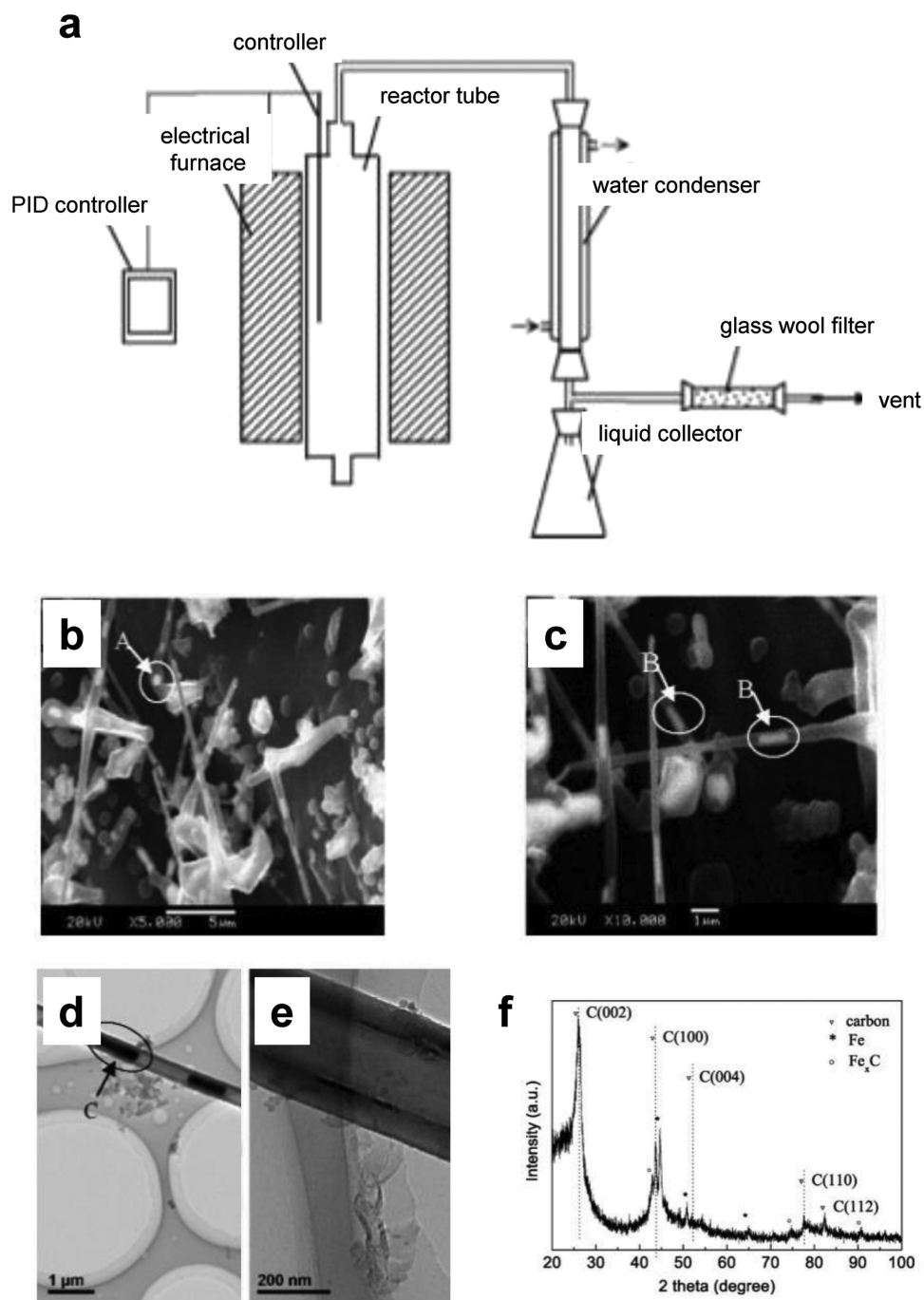


Figure 19. a) Schematics of fixed reactor system for pyrolytic synthesis of CNTs. SEM images of CNTs with b) nanoparticles and c) nanorods. TEM images of d) CNTs and e) their magnified one. f) XRD pattern of the synthesized CNTs. Reproduced with permission.^[85] Copyright 2010, Elsevier.

from polymer wastes had a conductivity of 43 S m^{-1} at room temperature and 72 S m^{-1} at 60°C (Figure 22e). They were used in water purification as a practical application (Figure 22f). When the CNTs are added to a solution of gold NPs, they adsorb to the surface of CNTs and can be removed from solution, thereby purifying the water.

Plastic wastes were also converted to CNTs by CVD using a Ni catalyst, by a process in which all synthesis steps occur in

one chamber (Figure 23a).^[91] During the pyrolysis process, a waste precursor decomposes and diffuses to the catalyst surface. After the catalyst becomes supersaturated with carbon species, precipitation occurs, and CNTs nucleate and growth. Raman spectra of CNTs were affected by growth temperature (Figure 23b). As growth temperature increased, I_G and I_{2D} increased, whereas I_D decreased; these trends reveal that the increase of growth temperature caused a decrease in the

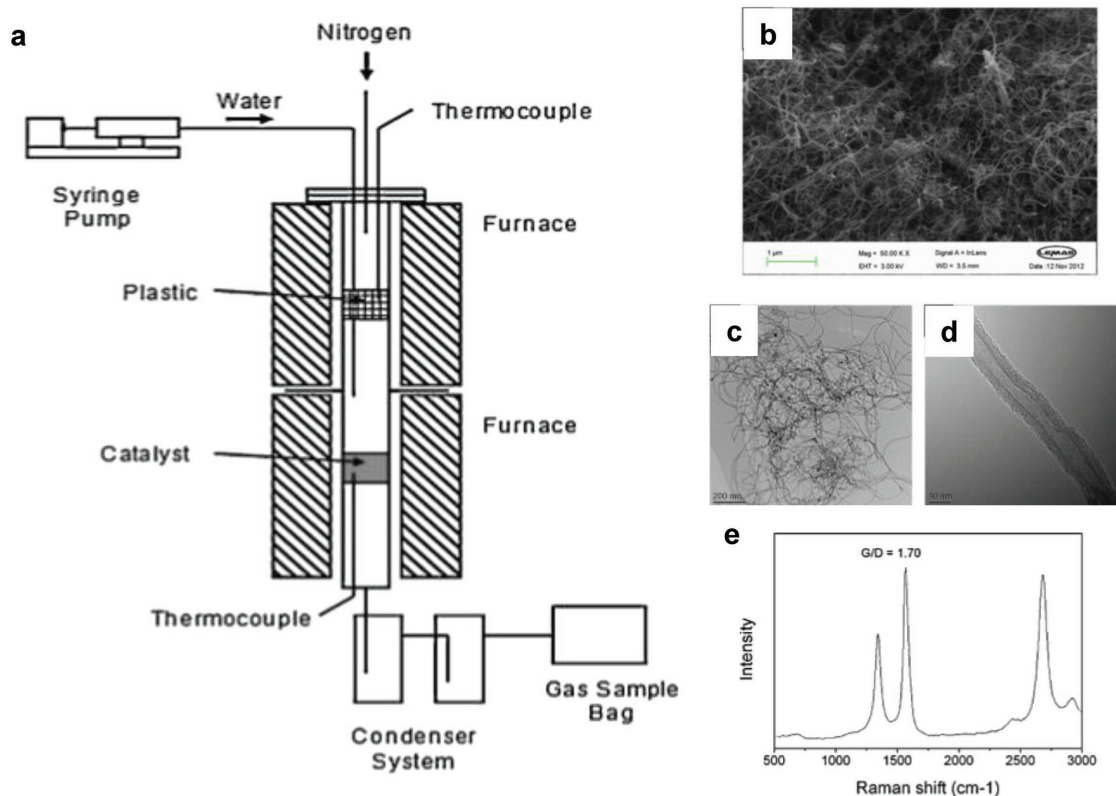


Figure 20. a) Schematics of pyrolytic gasification reactors for CNTs synthesis. b) SEM images and c,d) TEM images of the carbon deposits derived from LDPE. e) Raman spectra of carbon deposits derived from LDPE. Reproduced with permission.^[86] Copyright 2014, Elsevier.

density of defects and amorphous carbon, and improvement in CNT purity. XRD detected the presence of graphite structure (26°, 42°, 55°, and 77°) and Ni (44°) (Figure 23c). SEM image indicated that derived CNTs had diameter ≈20 nm and lengths of several tens to a hundreds of micrometers (Figure 23d), which well coincides with TEM and HR-TEM results (Figure 23e,f). OT of prepared CNTs was sufficiently high (>85% at 550 nm) (Figure 23g), which suggests that

CNTs derived from the plastic waste can be used in transparent electrodes.

3.2.2. Plasma Treatment

Arc discharge has been evaluated as a simple and cost-effective process to synthesize CNTs from carbon waste.^[93] Waste

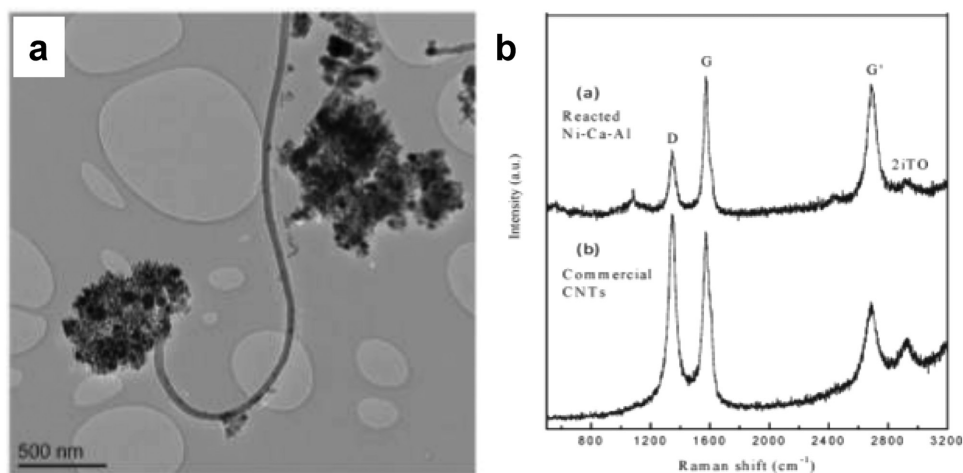


Figure 21. a) TEM images and b) Raman spectra of carbon deposits derived from plastic wastes. Reproduced with permission.^[87] Copyright 2012, Royal Society of Chemistry.

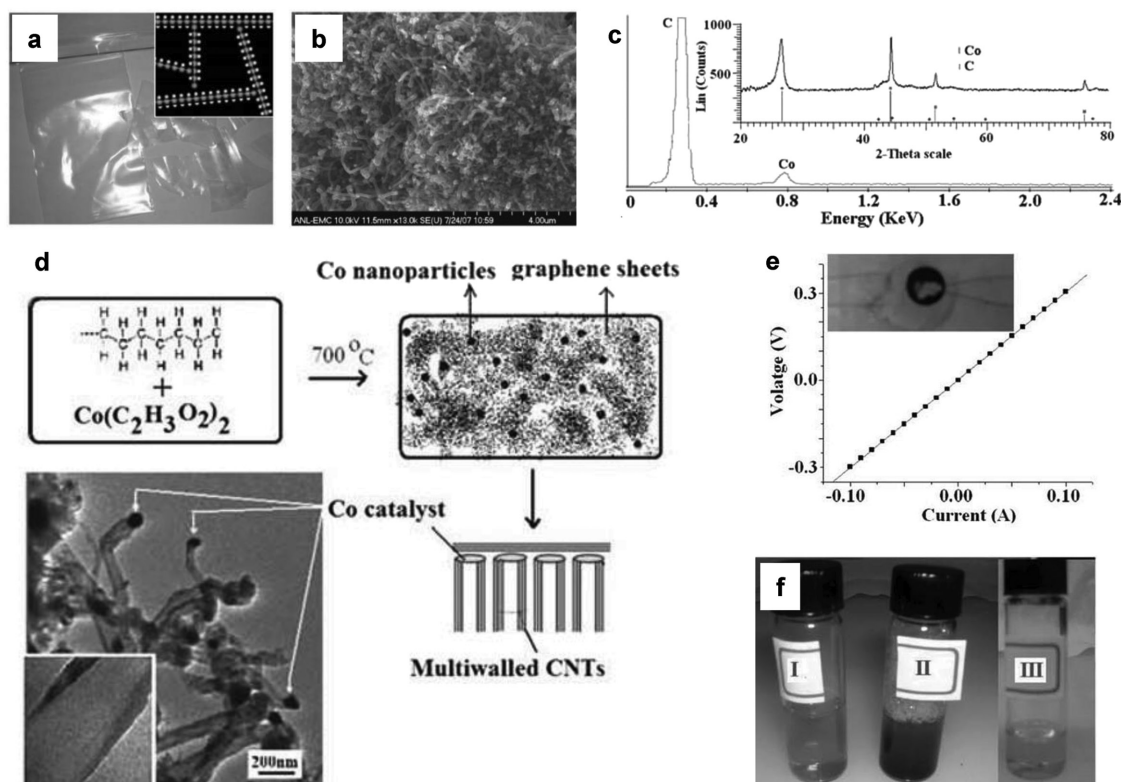


Figure 22. a) Photograph of LDPE (inset: chemical arrangement of polyethylene groups in LDPE). b) SEM images of CNTs obtained from LDPE. c) Energy-dispersive spectra of CNTs from LDPE (inset: XRD pattern of CNTs). d) Schematics of growth mechanism of CNTs. e) Current–voltage characteristics of LDPE-derived CNTs. f) Photograph of gold nanoparticle removal in solution by CNT purification. Reproduced with permission.^[90] Copyrights 2010, Royal Society of Chemistry.

PETs were first pyrolyzed under N_2 atmosphere to form polymer char, then subjected to an arc discharge (Figure 24a). The arc discharge raises the temperature of the anode tip to $\approx 3000^\circ\text{C}$ which is high enough to generate plasma, then soot forms in region I (Figure 24a). This soot includes fine CNTs (Figure 24b,c) that have an average diameter of ≈ 364 nm, and lengths of several micrometers. During the arc discharge, the anode is consumed and deposited onto the cathode as soot, so a mixture of CNTs and carbon particles formed on cathode surface (Figure 24d). Y-shaped CNTs were also obtained in anode soot (Figure 24e), they were longer but thinner (≈ 95 nm) than the CNTs in region I. Soot at the cathode contained more straight CNTs rather than the soot in the anode, so the density of defects in CNTs was lower at the cathode than those in CNTs at the anode (Figure 24f). This result coincides well with Raman spectra, which showed lower I_D/I_G in CNTs from the cathode than in CNTs from the anode (Figure 24g); temperature has a strong influence on the quality of synthesized CNTs, so this difference may be a result of the temperature during the arc discharge being higher at the cathode than at the anode. In XRD results, the peak at 26.26° , which corresponds to (002) plane, was sharper and narrower in CNTs from the cathode than in CNTs from the anode. This result means that graphitization was higher in CNTs from the cathode than in CNTs from the anode.

CNTs can be synthesized by arc discharge with fullerene waste soot as the precursor, with Ni and Y_2O_3 catalysts.^[94]

Fullerene soot was mixed with the catalyst, carbonized at 900°C , and then subjected to arc discharge to form CNTs. The resulting carbon deposit includes numerous filament-structured CNTs, which are tangled to form macronetworks (Figure 25a). The CNTs tended to aggregate (Figure 25b); this behavior can be attributed to van der Waals forces between them. The CNTs had diameters from 1.2 to 2.0 nm, and were capped by hemispherical structures (Figure 25c,d). Fullerene precursor yielded more CNTs than did the control treatment that used graphite as a precursor; this difference may occur because chemical bonding is more easily broken in amorphous carbon in fullerene soot than in graphite, and that fullerene fragments can be used directly as seeds for CNT growth. In Raman spectra, I_D/I_G was higher in fullerene-derived CNTs than in graphite-derived CNTs (Figure 25e); this difference agrees well with the higher yield of fullerene-derived CNTs than of graphite-derived CNTs. Raman shift in the region of $100\text{--}200\text{ cm}^{-1}$ indicates the radial breathing mode of CNTs, which is related to their diameter. The XRD pattern of fullerene soot obtained from the anode showed a broad peak in (002) plane with sharp peaks of Y_2O_3 and cubic Ni (Figure 25f). This pattern indicates that turbostratic stacking of carbons is dominant in the carbon deposits, and that the metallic catalysts contaminated the CNTs. A growth model of CNTs from fullerene-based soot was depicted in Figure 25g. First, the arc discharge vaporizes carbon, which aggregates to form fullerene-like fragments.

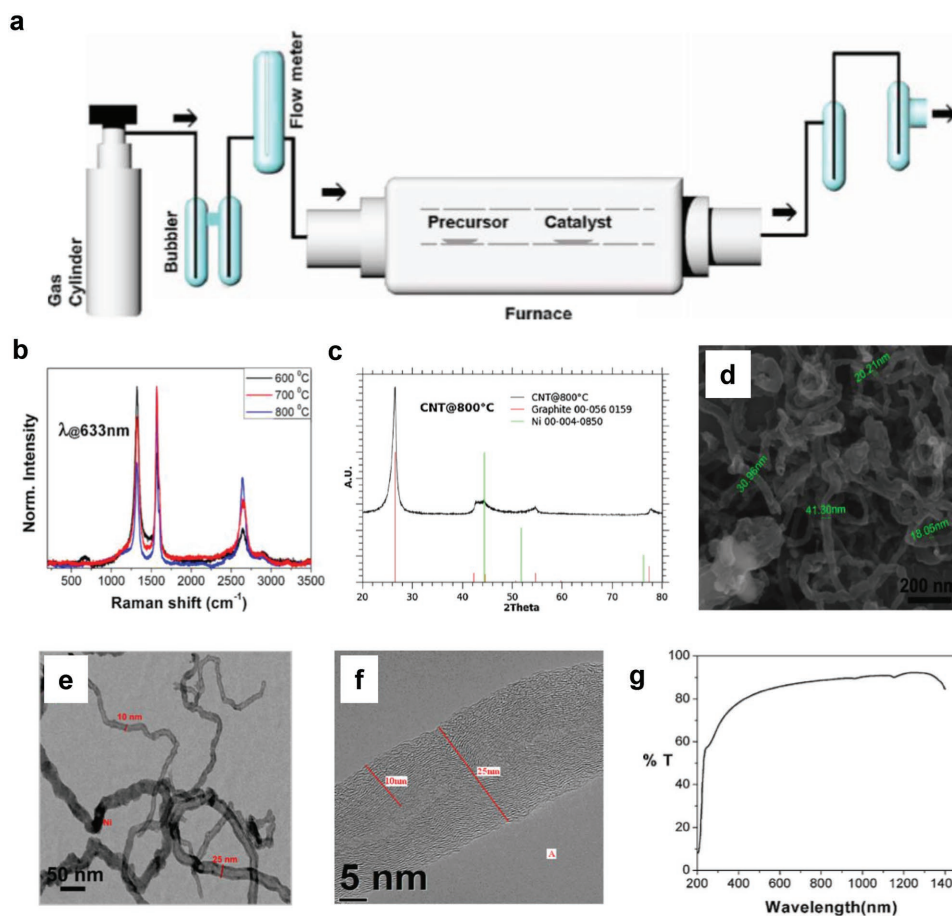


Figure 23. a) Schematics of CVD chambers for CNTs derived from polypropylene. b) Raman spectra of CNTs synthesized at various temperatures. c) XRD pattern of CNTs synthesized at 800 °C. d) SEM and e,f) TEM images of synthesized CNTs. g) Optical transmittance of prepared CNTs. Reproduced with permission.^[91] Copyrights 2012, Elsevier.

Metal atoms exist as gas phase at this stage because arc discharge causes high temperature. After temperature decreases, gaseous metal atoms condense to form particles, and are supersaturated by the covered carbon. Edges of fullerene-like fragments tend to bond to metal particles to eliminate dangling bonds; these aggregates provide nucleation sites for CNT growth. When the temperature is near the eutectic temperature, CNTs grow by consuming carbon from precipitated metal particles or amorphous carbon that surrounds them.

4. Discussion and Perspectives

This work has reviewed recent progress in synthesis of graphene and CNTs from carbon wastes. This process can recycle inexpensive precursors to value-added products that have outstanding electronic, optical, and mechanical properties and are therefore regarded as promising materials for use in nanoelectronics and optoelectronics. Various methods have been developed to convert graphene and CNTs from carbon waste; examples include pyrolysis, CVD, and plasma treatment.

CNTs are obtained from carbon waste mainly by pyrolysis using additives that contain metallic elements. To the best of our knowledge, the CNTs obtained are of limited quality, and their

electrical properties (i.e., electrical conductivity and electron mobility) are poor; thus, the practical applications of these CNTs are strongly limited to water purification and molecular separation membrane,^[90] in which high-quality CNTs are not necessary.

Graphene is obtained from carbon waste mainly by pyrolysis, or by CVD method with additives or metal catalysts. Pyrolysis yields graphene that is of limited quality, so its electrical properties are still poor and its practical application is also limited to water purification, and catalyst of oxygen reduction. Graphene obtained by plasma treatment is also of low quality, so its applications (biosensing) are limited as well.^[59] However, the CVD method that uses solid carbon waste decomposes the solid precursor, leaving carbon-containing gaseous molecules, and these are converted into the graphene via catalytic reaction on metal surface. Thus, graphene obtained by CVD from carbon waste showed substantially improved quality, with $R_{sh} < 1000 \Omega \text{ sq}^{-1}$. This graphene has been used as an electrode in practical electronic applications (i.e., FETs). Graphene derived from carbon waste had lower R_C than a conventional Au electrode in FETs.^[33] Furthermore, synthesis in a CVD furnace can form a dielectric/graphene layer directly from inexpensive carbon sources; this layer has been used in FETs.^[58] These reports demonstrated the possibility of using waste-derived graphene in practical electronics.

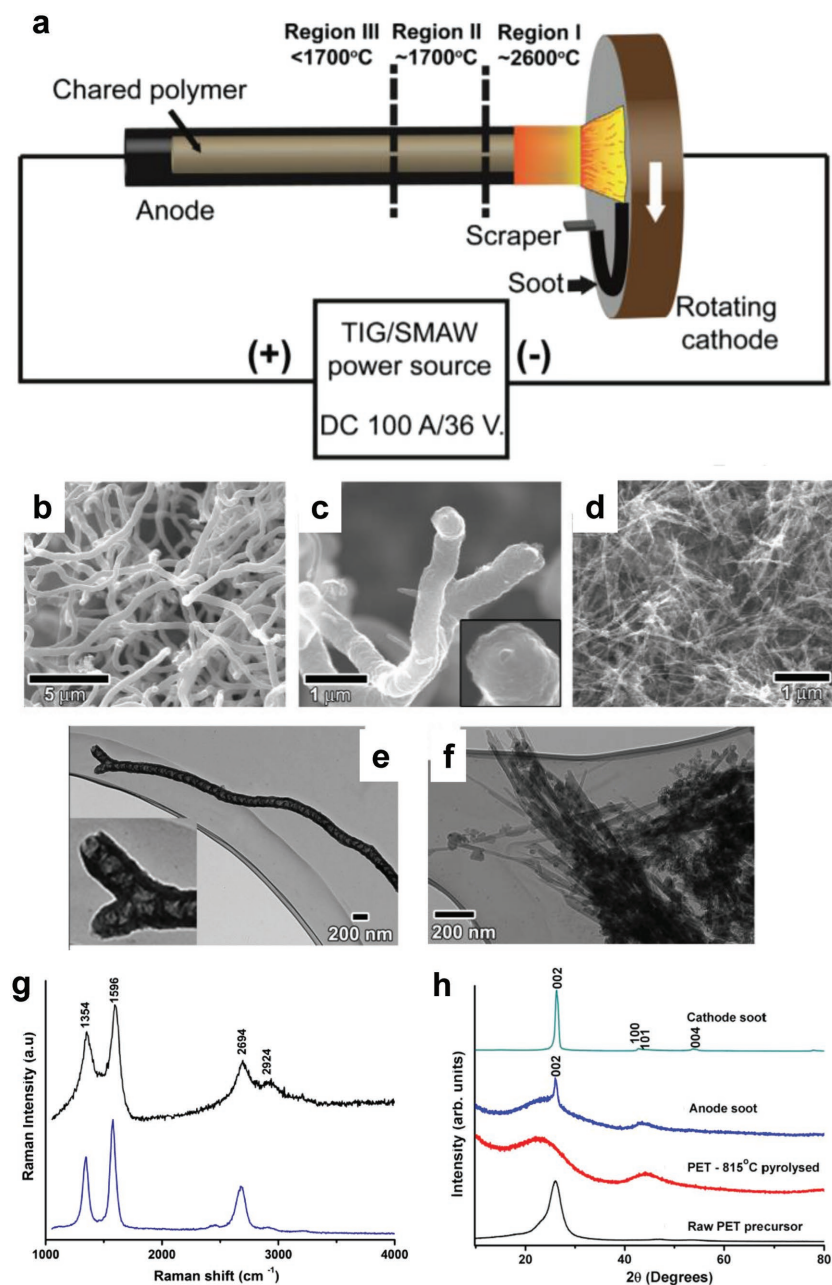


Figure 24. a) Schematics of CNTs from plastic wastes using the arc discharge method. SEM images of b) CNTs obtained from anode soot. c) CNTs at higher magnification. d) CNTs obtained from cathode soot. TEM images of CNTs from e) anode soot and f) cathode soot. g) Raman spectra of CNTs synthesized in anode soot (black) and cathode soot (blue). h) XRD patterns of raw PET (black), pyrolyzed PET (red), anode soot (blue), and cathode soot (dark cyan). Reproduced with permission.^[93] Copyrights 2014, Elsevier.

There were several reports that graphene derived from carbon wastes or inexpensive polymeric source (e.g., cookie, grass, plastic, PMMA) showed high quality, which is comparable to those derived from purified carbon gases.^[55,63] However, graphene and CNTs derived from carbon waste usually have lower quality than those synthesized from purified gaseous precursors, and as a result have degraded electrical properties. Nevertheless, practical application of the waste-derived graphene and CNTs is of primary

importance due to its cost competitiveness and eco friendliness. Especially, waste-derived graphene usually formed a 3D structure rather than planar structure;^[53,59] this 3D may be applicable in stretchable electronics.^[95,96]

Functionality of graphene and CNTs can be dependent on their specific characteristics. Because water purification occurs on the surface of the carbon materials, it should have high surface-to-volume ratio for efficient purification reaction.^[37] Carbon materials in biosensors or supercapacitors work via surface-reaction during the operation.^[59] For these purpose, recycling from carbon waste should aim to synthesize graphene and CNTs of 3D structure or porous structure. On the other hands, graphene and CNTs, to be used in electrodes of flexible optoelectronics, should have high electrical conductivity with uniform surface. High conductivity is important to achieve high efficiency of flexible organic optoelectronic devices, and high degree of sp^2 -hybridization would obtain graphene and CNTs of high conductivity. During the device operation, uniform surface of CNTs and graphene electrode in organic optoelectronics can prevent leakage current, which severely degrade the device stability.

Before use of waste-derived graphene and CNTs is practical in electronics, improvements are required in i) quality, ii) electrical properties, and iii) productivity. Most reports indicate that the electrical properties of the graphene and CNTs are far inferior to those required for practical applications; exceptions include several papers about graphene derived from catalytic decomposition of solid waste. Practical applications of graphene and CNTs in optoelectronics are still in the early stage. Graphene and CNTs from carbon wastes must be of high quality (i.e., high degree of sp^2 -hybridized carbon network) and have high electrical conductivity with uniform surface if it is to be appropriate for electronic applications. The quality of graphene and CNTs could be improved by modifying several factors such as growth temperature, injection rate of precursors, and choice of catalyst. Similar to the previous research about high-quality graphene derived from carbon wastes,^[55,63] recycling from inexpensive

carbon precursors which are thermally decomposed from polymeric sources into carbon-containing small molecules and have gas-phase reaction can yield high-quality graphene.

The electrical properties of graphene and CNTs must be controlled before they can have practical applications in optoelectronics. Graphene has a work function (WF) of ≈ 4.4 eV, and CNTs have a WF of ≈ 4.7 eV, so the electrode and adjacent organic layer are separated by a large energy difference, which

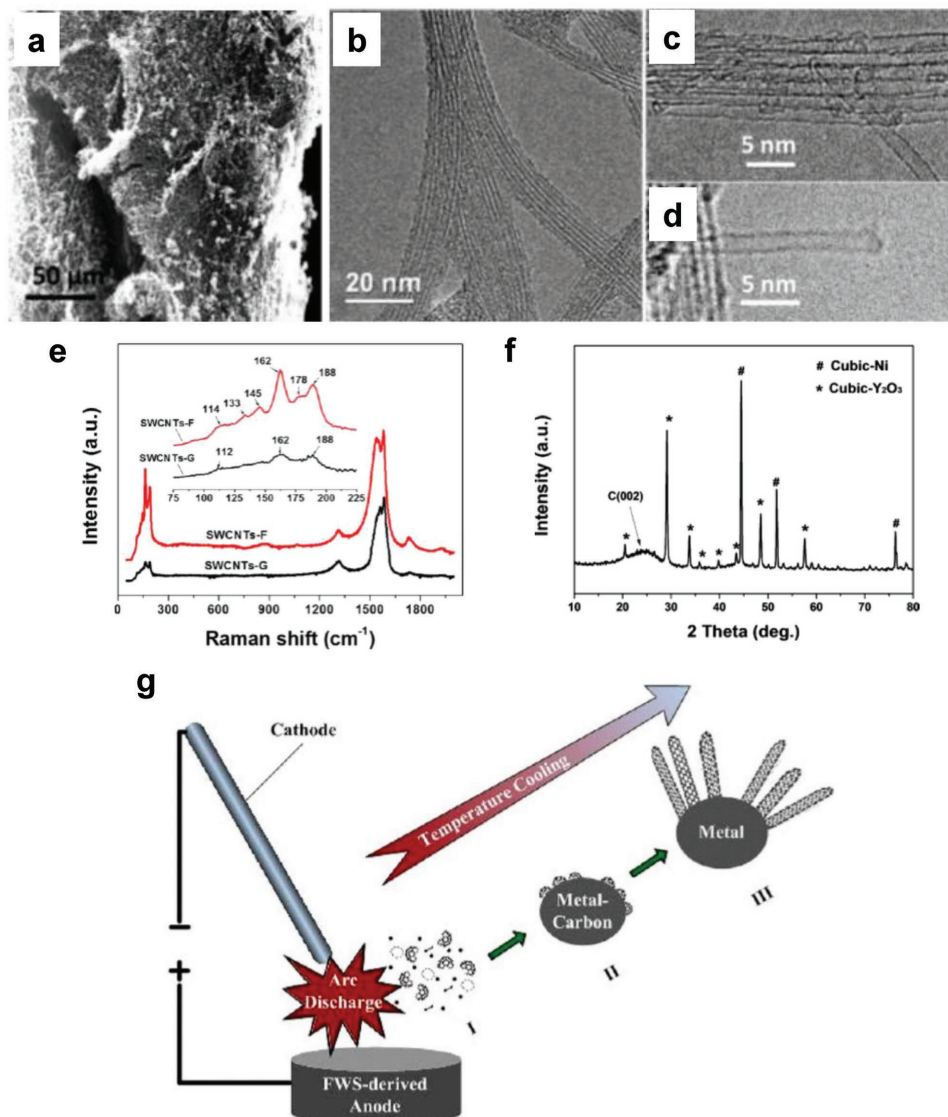


Figure 25. a) SEM, b) TEM, and c,d) high-resolution TEM images of CNTs derived from fullerene soot. e) Raman spectra of CNTs derived from graphite (black) and fullerene soot (red). f) XRD patterns of CNTs derived from fullerene soot. g) Schematics of growth of CNTs from fullerene-derived waste during arc discharge. Reproduced with permission.^[94] Copyrights 2014, American Chemical Society.

impedes charge injection. In addition, the conductivities of graphene and CNTs are still inferior to that of conventional indium–tin oxide, which has $R_{sh} < 50 \, \Omega \, \text{sq}^{-1}$. During the operation of optoelectronics, low conductivity of the electrode reduces current flow through the device, and limits its electronic characteristics. Chemical doping can modulate the electrical properties of graphene and CNTs. By using carbon wastes that include heteroatoms (i.e., B and N) as a precursor for graphene or CNT, these atoms can replace carbon in sp^2 -hybridized carbon networks. B atoms in carbon networks induce a p-type doping effect, and N atoms in carbon networks induces n-type doping effect.^[97] Post-treatment of chemical dopants on synthesized graphene or CNTs can also induce doping effects. Chemical dopants that spontaneously withdraw or donate electrons of graphene and CNTs cause p-type doping, or n-type doping effect, respectively. Especially, these approaches do not

break the sp^2 -hybridization of carbon networks, and therefore do not degrade the conductivity of graphene or CNTs.

Productivity must be improved as well, before practical applications are possible. To date, synthesis of graphene or CNTs from carbon wastes have been limited to laboratory scale. Also, their yield is far below a commercializable level. We present the two major requirements that must be met to realize a scalable recycling process: i) applying high temperature to a large area, and ii) depositing precursors uniformly over a large area.

CVD graphene synthesis on a large area ($\approx 30 \, \text{in.}$) has been achieved using a roll-to-roll production system.^[98] The growth temperature was $\approx 1000 \, ^\circ\text{C}$, which is significantly high compared to those of the pyrolysis and CVD processes that have been presented in this review. We expect that this technology to apply high temperature uniformly at large scale can be adapted to recycling of carbon wastes into graphene or CNTs.

Large-area solution-processed electronics have been successfully demonstrated by various groups.^[99] Methods to deposit the solution and to prepare patterns over a large area have been developed, and several companies already fabricate large-area solution-processed optoelectronics. Waste precursor, which can mostly be prepared as solution forms by dissolving appropriate solvents, can be deposited uniformly over large area by using conventional solution printing technology; again, we expect that these methods can be adapted to recycling of carbon wastes into graphene or CNTs.

Use of waste-derived graphene or CNTs in electronics has been confined to electrodes in FETs, which have much simpler structure than OLEDs or OSCs. To broaden the electronic applications from FETs to optoelectronics (e.g., OLEDs and OSCs), the graphene or CNT layer must be smooth and have high transparency, in addition to low R_{sh} and appropriate WF. Optoelectronic devices are usually composed of organic layers that have thicknesses of several tens of nanometers. Rough surface induces leakage current during the operation of optoelectronic devices, which reduces the stability of device operation. High transparency is another requirement of graphene or CNTs for use in optoelectronics, because light absorption of the device should be minimized.

Further development of graphene and CNTs derived from carbon wastes should aim to increase the quality of graphene and CNTs, electrical properties and productivity. At the same time, development of a recycling process that yields graphene and CNTs with smooth surface and high transparency would facilitate use of waste-derived graphene and CNTs in nanoelectronics and optoelectronics. Ecological sustainability should also be considered. Graphene and CNTs would have low degradability and can be toxic, so methods to dispose of or recycle graphene and CNTs should also be developed.^[100]

Acknowledgements

S.-J.K. and H.-K.S. contributed equally to this work. This work was supported by the National Research Foundation of Korea (NRF) grant (NRF-2016R1A3B1908431) funded by the Korean government (Ministry of Science and ICT).

Conflict of Interest

The authors declare no conflict of interest.

Keywords

carbon nanotubes, carbon waste, flexible electronics, graphene, recycling

Received: January 31, 2018

Revised: March 20, 2018

Published online: June 14, 2018

[1] J. N. Chheda, G. W. Huber, J. A. Dumesic, *Angew. Chem., Int. Ed.* **2007**, *46*, 7164.

[2] N. Miskolczi, A. Angyal, L. Bartha, I. Valkai, *Fuel Process. Technol.* **2009**, *90*, 1032.

- [3] K. S. Novoselov, A. K. Geim, S. V. Morozov, D. Jiang, Y. Zhang, S. V. Dubonos, I. V. Grigorieva, A. A. Firsov, *Science* **2004**, *306*, 666.
- [4] A. K. Geim, K. S. Novoselov, *Nat. Mater.* **2007**, *6*, 183.
- [5] J. A. Rogers, *Nat. Nanotechnol.* **2008**, *3*, 254.
- [6] Y. B. Zhang, Y. W. Tan, H. L. Stormer, P. Kim, *Nature* **2005**, *438*, 201.
- [7] M. I. Katsnelson, *Mater. Today* **2007**, *10*, 20.
- [8] K. S. Novoselov, Z. Jiang, Y. Zhang, S. V. Morozov, H. L. Stormer, U. Zeitler, J. C. Maan, G. S. Boebinger, P. Kim, A. K. Geim, *Science* **2007**, *315*, 1379.
- [9] Z. Jiang, Y. Zhang, H. L. Stormer, P. Kim, *Phys. Rev. Lett.* **2007**, *99*, 106802.
- [10] E. P. S. Tan, C. T. Lim, *Compos. Sci. Technol.* **2006**, *66*, 1102.
- [11] Z. Deng, E. Yenilmez, A. Reilein, J. Leu, H. Dai, K. A. Moler, *Appl. Phys. Lett.* **2006**, *88*, 23119.
- [12] H. Huang, R. Maruyama, K. Noda, H. Kajiura, K. Kadono, *J. Phys. Chem. B* **2006**, *110*, 7316.
- [13] P. Laborde-Lahoz, W. Maser, T. Martínez, A. Benito, T. Seeger, P. Cano, R. G. de Villoria, A. Miravete, *Mech. Adv. Mater. Struct.* **2005**, *12*, 13.
- [14] M. S. Dresselhaus, H. Dai, *MRS Bull.* **2004**, *29*, 237.
- [15] A. Javey, J. Guo, Q. Wang, M. Lundstrom, H. Dai, *Nature* **2003**, *424*, 654.
- [16] B. Obradovic, R. Kotlyar, F. Heinz, P. Matagne, T. Rakshit, M. D. Giles, M. A. Stettler, D. E. Nikonov, *Appl. Phys. Lett.* **2006**, *88*, 142102.
- [17] Y. Ouyang, Y. Yoon, J. K. Fodor, J. Guo, *Appl. Phys. Lett.* **2006**, *89*, 203107.
- [18] T.-H. Han, H. Kim, S.-J. Kwon, T.-W. Lee, *Mater. Sci. Eng., R* **2017**, *118*, 1.
- [19] A. Southard, V. Sangwan, J. Cheng, E. D. Williams, M. S. Fuhrer, *Org. Electron.* **2009**, *10*, 1556.
- [20] J. Park, W. H. Lee, S. Huh, S. H. Sim, S. B. Kim, K. Cho, B. H. Hong, K. S. Kim, *J. Phys. Chem. Lett.* **2011**, *2*, 841.
- [21] M. W. Rowell, M. A. Topinka, M. D. McGehee, H.-J. Prall, G. Dennler, N. S. Sariciftci, L. Hu, G. Gruner, *Appl. Phys. Lett.* **2006**, *88*, 233506.
- [22] H. Kim, S.-H. Bae, T.-H. Han, K.-G. Lim, J.-H. Ahn, T.-W. Lee, *Nanotechnology* **2014**, *25*, 14012.
- [23] H. Kim, J. Byun, S.-H. Bae, T. Ahmed, J.-X. Zhu, S.-J. Kwon, Y. Lee, S.-Y. Min, C. Wolf, H.-K. Seo, J.-H. Ahn, T.-W. Lee, *Adv. Energy Mater.* **2016**, *6*, 1600172.
- [24] K. Kim, S.-H. Bae, C. T. Toh, H. Kim, J. H. Cho, D. Whang, T.-W. Lee, B. Özyilmaz, J.-H. Ahn, *ACS Appl. Mater. Interfaces* **2014**, *6*, 3299.
- [25] T.-H. Han, Y. Lee, M.-R. Choi, S.-H. Woo, S.-H. Bae, B. H. Hong, J.-H. Ahn, T.-W. Lee, *Nat. Photonics* **2012**, *6*, 105.
- [26] C. M. Aguirre, S. Auvray, S. Pigeon, R. Izquierdo, P. Desjardins, R. Martel, *Appl. Phys. Lett.* **2006**, *88*, 183104.
- [27] T.-H. Han, S.-J. Kwon, N. Li, H.-K. Seo, W. Xu, K. S. Kim, T.-W. Lee, *Angew. Chem., Int. Ed.* **2016**, *55*, 6197.
- [28] J. Lee, T.-H. Han, M.-H. Park, D. Y. Jung, J. Seo, H.-K. Seo, H. Cho, E. Kim, J. Chung, S.-Y. Choi, T.-S. Kim, T.-W. Lee, S. Yoo, *Nat. Commun.* **2016**, *7*, 11791.
- [29] T.-H. Han, M.-H. Park, S.-J. Kwon, S.-H. Bae, H.-K. Seo, H. Cho, J.-H. Ahn, T.-W. Lee, *NPG Asia Mater.* **2016**, *8*, e303.
- [30] J. Kong, A. M. Cassell, H. Dai, *Chem. Phys. Lett.* **1998**, *292*, 567.
- [31] J.-F. Colomer, C. Stephan, S. Lefrant, G. Van Tendeloo, I. Willems, Z. Kónya, A. Fonseca, C. Laurent, J. B. Nagy, *Chem. Phys. Lett.* **2000**, *317*, 83.
- [32] N. Arora, N. N. Sharma, *Diamond Relat. Mater.* **2014**, *50*, 135.
- [33] H.-K. Seo, T.-S. Kim, C. Park, W. Xu, K. Baek, S.-H. Bae, J.-H. Ahn, K. Kim, H. C. Choi, T.-W. Lee, *Sci. Rep.* **2015**, *5*, 16710.
- [34] S. Sharma, G. Kalita, R. Hirano, S. M. Shinde, R. Papon, H. Ohtani, M. Tanemura, *Carbon* **2014**, *72*, 66.

- [35] F. Pan, J. Jin, X. Fu, Q. Liu, J. Zhang, *ACS Appl. Mater. Interfaces* **2013**, 5, 11108.
- [36] S. S. Shams, L. S. Zhang, R. Hu, R. Zhang, J. Zhu, *Mater. Lett.* **2015**, 161, 476.
- [37] S. Sen Gupta, T. S. Sreeprasad, S. M. Maliyekkal, S. K. Das, T. Pradeep, *ACS Appl. Mater. Interfaces* **2012**, 4, 4156.
- [38] K. I. Bolotin, K. J. Sikes, Z. Jiang, M. Klima, G. Fudenberg, J. Hone, P. Kim, H. L. Stormer, *Solid State Commun.* **2008**, 146, 351.
- [39] R. R. Nair, P. Blake, A. N. Grigorenko, K. S. Novoselov, T. J. Booth, T. Stauber, N. M. R. Peres, A. K. Geim, *Science* **2008**, 320, 1308.
- [40] C. Lee, X. Wei, J. W. Kysar, J. Hone, *Science* **2008**, 321, 385.
- [41] S. Iijima, *Nature* **1991**, 354, 56.
- [42] J. Prasek, J. Drbohlavova, J. Chomoucka, J. Hubalek, O. Jasek, V. Adam, R. Kizek, *J. Mater. Chem.* **2011**, 21, 15872.
- [43] V. N. Popov, *Mater. Sci. Eng., R* **2004**, 43, 61.
- [44] T. Dürkop, S. A. Getty, E. Cobas, M. S. Fuhrer, *Nano Lett.* **2004**, 4, 35.
- [45] M.-F. Yu, B. S. Files, S. Arepalli, R. S. Ruoff, *Phys. Rev. Lett.* **2000**, 84, 5552.
- [46] Z. Wu, Z. Chen, X. Du, J. M. Logan, J. Sippel, M. Nikolou, K. Kamaras, J. R. Reynolds, D. B. Tanner, A. F. Hebard, A. G. Rinzler, *Science* **2004**, 305, 1273.
- [47] M. J. Allen, V. C. Tung, R. B. Kaner, *Chem. Rev.* **2010**, 110, 132.
- [48] M. Yi, Z. Shen, *J. Mater. Chem. A* **2015**, 3, 11700.
- [49] W. S. Hummers, R. E. Offeman, *J. Am. Chem. Soc.* **1958**, 80, 1339.
- [50] S. Gilje, S. Han, M. Wang, K. L. Wang, R. B. Kaner, *Nano Lett.* **2007**, 7, 3394.
- [51] X. Li, W. Cai, L. Colombo, R. S. Ruoff, *Nano Lett.* **2009**, 9, 4268.
- [52] K. S. Kim, Y. Zhao, H. Jang, S. Y. Lee, J. M. Kim, K. S. Kim, J. H. Ahn, P. Kim, J. Y. Choi, B. H. Hong, *Nature* **2009**, 457, 706.
- [53] A. K. Ray, R. K. Sahu, V. Rajinikanth, H. Bapari, M. Ghosh, P. Paul, *Carbon* **2012**, 50, 4123.
- [54] T. S. Sreeprasad, S. Sen Gupta, S. M. Maliyekkal, T. Pradeep, *J. Hazard. Mater.* **2013**, 246–247, 213.
- [55] G. Ruan, Z. Sun, Z. Peng, J. M. Tour, *ACS Nano* **2011**, 5, 7601.
- [56] S. H. Vijapur, D. Wang, G. G. Botte, *ECS Solid State Lett.* **2013**, 2, M45.
- [57] S.-J. Byun, H. Lim, G.-Y. Shin, T.-H. Han, S. H. Oh, J.-H. Ahn, H. C. Choi, T.-W. Lee, *J. Phys. Chem. Lett.* **2011**, 2, 493.
- [58] H.-K. Seo, K. Kim, S.-Y. Min, Y. Lee, C. E. Park, R. Raj, T.-W. Lee, *2D Mater.* **2017**, 4, 024001.
- [59] D. H. Seo, A. E. Rider, Z. J. Han, S. Kumar, K. (Ken) Ostrikov, *Adv. Mater.* **2013**, 25, 5638.
- [60] Q. Zhou, Z. Zhao, Y. Zhang, B. Meng, A. Zhou, J. Qiu, *Energy Fuels* **2012**, 26, 5186.
- [61] A. C. Ferrari, J. C. Meyer, V. Scardaci, C. Casiraghi, M. Lazzeri, F. Mauri, S. Piscanec, D. Jiang, K. S. Novoselov, S. Roth, A. K. Geim, *Phys. Rev. Lett.* **2006**, 97, 187401.
- [62] B. Shen, D. Lu, W. Zhai, W. Zheng, *J. Mater. Chem. C* **2013**, 1, 50.
- [63] Z. Sun, Z. Yan, J. Yao, E. Beitler, Y. Zhu, J. M. Tour, *Nature* **2010**, 468, 549.
- [64] A. K. Mishra, S. Ramaprabhu, *Desalination* **2011**, 282, 39.
- [65] Y. S. Ho, G. McKay, *Water Res.* **2000**, 34, 735.
- [66] K. P. Lisha, S. M. Maliyekkal, T. Pradeep, *Chem. Eng. J.* **2010**, 160, 432.
- [67] T. S. Sreeprasad, S. M. Maliyekkal, K. P. Lisha, T. Pradeep, *J. Hazard. Mater.* **2011**, 186, 921.
- [68] A. Das, S. Pisana, B. Chakraborty, S. Piscanec, S. K. Saha, U. V. Waghmare, K. S. Novoselov, H. R. Krishnamurthy, A. K. Geim, A. C. Ferrari, A. K. Sood, *Nat. Nanotechnol.* **2008**, 3, 210.
- [69] Y. Hao, Y. Wang, L. Wang, Z. Ni, Z. Wang, R. Wang, C. K. Koo, Z. Shen, J. T. L. Thong, *Small* **2010**, 6, 195.
- [70] A. W. Robertson, J. H. Warner, *Nano Lett.* **2011**, 11, 1182.
- [71] A. Reina, X. Jia, J. Ho, D. Nezich, H. Son, V. Bulovic, M. S. Dresselhaus, J. Kong, *Nano Lett.* **2009**, 9, 30.
- [72] S. Lee, G. Jo, S.-J. Kang, G. Wang, M. Choe, W. Park, D.-Y. Kim, Y. H. Kahng, T. Lee, *Adv. Mater.* **2011**, 23, 100.
- [73] S. Lee, S.-J. Kang, G. Jo, M. Choe, W. Park, J. Yoon, T. Kwon, Y. H. Kahng, D.-Y. Kim, B. Hun Lee, T. Lee, *Appl. Phys. Lett.* **2011**, 99, 83306.
- [74] C. Wang, Y. Zhou, L. He, T.-W. Ng, G. Hong, Q.-H. Wu, F. Gao, C.-S. Lee, W. Zhang, *Nanoscale* **2013**, 5, 600.
- [75] V. C. Sundar, J. Zaumseil, V. Podzorov, E. Menard, R. L. Willett, T. Someya, M. E. Gershenson, J. A. Rogers, *Science* **2004**, 303, 1644.
- [76] Y. Wu, T. Zhang, F. Zhang, Y. Wang, Y. Ma, Y. Huang, Y. Liu, Y. Chen, *Nano Energy* **2012**, 1, 820.
- [77] K. Bazaka, M. V. Jacob, K. (Ken) Ostrikov, *Chem. Rev.* **2016**, 116, 163.
- [78] J. R. Miller, R. A. Outlaw, B. C. Holloway, *Science* **2010**, 329, 1637.
- [79] A. E. Rider, S. Kumar, S. A. Furman, K. (Ken) Ostrikov, *Chem. Commun.* **2012**, 48, 2659.
- [80] T. W. Ebbesen, P. M. Ajayan, *Nature* **1992**, 358, 220.
- [81] M. Kundrapu, J. Li, A. Shashurin, M. Keidar, *J. Phys. D: Appl. Phys.* **2012**, 45, 315305.
- [82] C. E. Baddour, C. Briens, *Int. J. Chem. React. Eng.* **2005**, 3, R3.
- [83] J. Chrzanoska, J. Hoffman, A. Maholepszy, M. Mazurkiewicz, T. A. Kowalewski, Z. Szymanski, L. Stobinski, *Phys. Status Solidi* **2015**, 252, 1860.
- [84] M. Endo, K. Takeuchi, S. Igarashi, K. Kobori, M. Shiraishi, H. W. Kroto, *J. Phys. Chem. Solids* **1993**, 54, 1841.
- [85] C. Quan, A. Li, N. Gao, *J. Hazard. Mater.* **2010**, 179, 911.
- [86] J. C. Acomb, C. Wu, P. T. Williams, *Appl. Catal., B* **2014**, 147, 571.
- [87] C. Wu, Z. Wang, L. Wang, P. T. Williams, J. Huang, *RSC Adv.* **2012**, 2, 4045.
- [88] C. Wu, M. A. Nahil, N. Miskolczi, J. Huang, P. T. Williams, *Environ. Sci. Technol.* **2014**, 48, 819.
- [89] C. Wu, Z. Wang, P. T. Williams, J. Huang, *Sci. Rep.* **2013**, 3, 2742.
- [90] V. G. Pol, P. Thiyagarajan, *J. Environ. Monit.* **2010**, 12, 455.
- [91] N. Mishra, G. Das, A. Ansaldo, A. Genovese, M. Malerba, M. Povia, D. Ricci, E. Di Fabrizio, E. Di Zitti, M. Sharon, M. Sharon, *J. Anal. Appl. Pyrolysis* **2012**, 94, 91.
- [92] T. Altalhi, T. Kumeria, A. Santos, D. Losic, *Carbon* **2013**, 63, 423.
- [93] A. Joseph Berkman, M. Jagannatham, S. Priyanka, P. Haridoss, *Waste Manag.* **2014**, 34, 2139.
- [94] C. Hu, C. Yu, M. Li, X. Fan, J. Yang, P. Zhang, S. Wang, Z. Zhao, J. Qiu, *ACS Sustainable Chem. Eng.* **2014**, 2, 14.
- [95] N. Liu, A. Chortos, T. Lei, L. Jin, T. R. Kim, W.-G. Bae, C. Zhu, S. Wang, R. Pfattner, X. Chen, R. Sinclair, Z. Bao, *Sci. Adv.* **2017**, 3, e1700159.
- [96] T. Chen, Y. Xue, A. K. Roy, L. Dai, *ACS Nano* **2014**, 8, 1039.
- [97] L. S. Panchakarla, K. S. Subrahmanyam, S. K. Saha, A. Govindaraj, H. R. Krishnamurthy, U. V. Waghmare, C. N. R. Rao, *Adv. Mater.* **2009**, 21, 4726.
- [98] S. Bae, H. Kim, Y. Lee, X. Xu, J.-S. Park, Y. Zheng, J. Balakrishnan, T. Lei, H. R. Kim, Y. I. Song, Y.-J. Kim, K. S. Kim, B. Ozyilmaz, J.-H. Ahn, B. H. Hong, S. Iijima, *Nat. Nanotechnol.* **2010**, 5, 574.
- [99] A. C. Arias, J. D. MacKenzie, I. McCulloch, J. Rivnay, A. Salleo, *Chem. Rev.* **2010**, 110, 3.
- [100] J. Zhao, Z. Wang, J. C. White, B. Xing, *Environ. Sci. Technol.* **2014**, 48, 9995.